University of Alberta

Distributed Parameter Control of Selective Catalytic Reduction (SCR) for Diesel-Powered Vehicles

by

Hallas Pakravesh

A thesis submitted to the Faculty of Graduate Studies and Research
in partial fulfillment of the requirements for the degree of

Master of Science
in
Process Control

Department of Chemical and Materials Engineering

Fall 2013
Edmonton, Alberta

Abstract

The main scope of this work is to design a distributed parameter control for SCR, which is modelled by using coupled hyperbolic and parabolic partial differential equations (PDEs). This is a boundary control problem where the control objectives are to reduce the amount of NO_x emissions and ammonia slip as far as possible. Two strategies are used to control SCR. The first strategy includes using the direct transcription (DT) as the open-loop control technique. The second strategy includes the design of a closed-loop control technique that uses a new numerical method developed in this work, which combines the method of characteristics and spectral decomposition, and the characteristic-based nonlinear model predictive control (CBNMPC) as the control algorithm. The results show that the designed advanced controllers are able to achieve very high control performance in terms of NO_x and ammonia slip reduction.

Acknowledgements

I would like to express my gratitude to my supervisor, Dr. Fraser Forbes, whose expertise, understanding, and patience, added considerably to my graduate experience. I appreciate his vast knowledge and skill in many areas (e.g., optimization and process control), and his assistance in writing this thesis. Also, I would like to thank the other members of my committee, Dr. Robert E. Hayes, and Dr. Stevan Dubljevic for the assistance they provided at all levels of the research project.

Contents

List of Figures

List of Tables

Chapter 1

Introduction

Diesel engines are one of the important power systems for vehicles and industrial equipment. Most of the heavy-duty trucks and buses are powered by diesel engines due to the extreme durability, high fuel-efficiency, and high torque output. Moreover, diesel engines can be easily repaired, and the operation of diesel engines is not expensive [1, 2].

Diesel engines use a different combustion cycle compared to spark-ignition engines. Both cycles usually include four piston strokes of intake, compression, power, and exhaust; however, they differ in how the fuel is supplied and ignited. In a typical gasoline spark-ignition engine without direct injection, the fuel is premixed with air and transferred into the cylinder during the intake stroke. The combustion begins when an electrical spark ignites the fuel-air mixture in the compression stroke. In a diesel engine, the fuel can be introduced into the combustion chamber under extremely high pressure during the intake or compression strokes, and the combustion begins without a spark, as the fuel-air mixture is spontaneously ignited with the high temperature and pressure of the cylinder. Contrary to the gasoline spark-ignition combustion, the diesel combustion does not require a uniform fuel-air mixture and can operate under a large amount of the excess air. The power output primarily is controlled by varying the amount of the fuel introduced into the engine. This kind of the power control process obviates the need for control of the airflow using the throttle [1].

While diesel engines have many advantages, there are some disadvantages of using them. First of all, they emit a large amount of particulate matter (PM) and oxides of nitrogen (NO_x) into the atmosphere. Furthermore, they emit toxic air pollutants that can have terrible effects on human health. Researchers have demonstrated that long-time exposure to diesel exhaust causes lung damage and respiratory problems, and in the worst case they may cause lung cancer. In addition, some environmental problems, (e.g., acid rain, ground-level ozone, and reduced visibility) can stem from pollutants emitted by diesel engines [2].

Today, practical emission control technologies can reduce the diesel exhaust emissions. The major diesel engine emission control technologies consist of the components designed to control particulate matter (PM), such as diesel oxidation catalysts (DOC), and diesel particulate filters (DPF), and the technologies designed to control the oxides of nitrogen (NO_x), such as exhaust gas recirculation (EGR), and selective catalytic reduction (SCR) [2].

Exhaust gas recirculation (EGR) is used to dilute the intake air using a fraction of the exhaust gas to lower the combustion temperature. Note that, lowering the combustion temperature can reduce the NO_x emissions in diesel engines. Also, EGR has the disadvantage of increasing the emission particulate matter. Variable geometry turbocharging (VGT), which delivers variable quantities of the pressurized air based on driving conditions, is efficient enough in reducing the PM emissions by maintaining lean combustion in the engine. Furthermore, the reduction of the compression ratios is also effective in lowering the combustion temperature. Diesel oxidation catalysts can effectively reduce the HC and CO emissions. The removal efficiency depends on catalyst composition, but up to 90% is possible for CO and HC. The effect of oxidation catalysts on particulate matter emissions is more complicated. This strongly depends on fuel and catalyst composition. A diesel particulate filter (DPF) is considered a particulate trap. Particles are trapped in the device, so over 80% of the particulate matter mass can be removed. The entrapped particles will increase the backpressure on the engine. The increase of the backpressure significantly reduces the fuel economy. Since high levels of the backpressure might be obtained quite quickly, it is necessary to remove the trapped particles periodically or continuously by a so-called regeneration technique. Diesel particulate filters are usually combined with EGR and SCR to achieve a significant NO_x and PM reduction. Selective catalytic reduction (SCR) is a technique to remove NO_x emissions by means of injecting a reducing agent.

Traditional aftertreatment systems, which are based on the three-way catalyst (TWC), demonstrate low performance under the excessive usage of oxygen [3, 4]. This has led to the development of novel technologies for NO_x removal in lean burn engines, which include: catalytic NO_x decomposition; NO_x storage reduction (NSR); and selective catalytic reduction (SCR) by ammonia or hydrocarbons. SCR is the only catalyst technology that is able to reduce diesel NO_x emissions to the Euro V (2008) and the JP 2005 NO_x limits, which are both set at a maximum 2 g/kwh for heavy-duty truck and bus engines. Thus, Urea-SCR has been selected by many manufacturers as the most suitable technology. Systems including SCR have been developed in the USA with the 2010 NO_x limit of 0.2 g/bhp-hr for heavy-duty engines [3, 5, 6].

There exist two commercial technologies in the automotive industry for the elimination of the NO_x emissions from lean-burn engines. The first one is the NO_x storage and reduction catalyst (NSRC) and the other is selective catalytic reduction of NO_x by NH_3 generated by a urea solution stored in a special tank (NH_3-SCR, urea-SCR). Note that, there is a possibility to combine the ammonia generation in the NSRC with the ammonia utilization in SCR. In fact, a combined diesel exhaust gas aftertreatment system consists of the NO_x storage and reduction catalyst (NSRC, called also lean NO_x trap, LNT) and the catalyst for the selective catalytic reduction of NO_x by NH_3 (NH_3-SCR). The system is often operated under the prevailing fuel-lean conditions in which the engine can run economically. During this phase, the NO_x emissions are adsorbed in NSRC. Short periods of fuel enrichment are applied periodically for the NSRC regeneration (reduction of the stored NO_x). The NO_x reduction under the controlled fuel-rich conditions in NSRC produces Ammonia as a by-product that is then adsorbed in the NH_3-SCR reactor located downstream. The adsorbed NH_3 is consequently used in SCR during the next fuel-lean period. The combination of NSRC and SCR is capable of obviating the need for an external NH_3 source (e.g., periodically re-filled the urea solution tank) that is necessary when SCR is used without NSRC.

SCR catalysts are produced from various ceramic materials, such as titanium oxide, active catalytic components that are usually either: oxides of base metals such as, vanadium, molybdenum and tungsten; zeolites; and various precious metals. Each catalyst component has advantages and disadvantages. Base metal catalysts have insufficient high thermal durability, but are less expensive and function very well at the operating temperatures that exist in industrial and utility boiler applications. The thermal durability is specifically important for automotive SCR applications that include diesel particulate filters with forced regeneration [7]. Zeolite catalysts have the ability to operate at higher temperatures (e.g. 900 K) and transient conditions of up to 1120 K. It should be noted that, nowadays, the main catalyst used in SCR is copper on zeolite [7, 8].

The optimal dosage of urea in SCR is the challenging issues in diesel-powered engines because the operating conditions of SCR during a drive cycle changes. Furthermore, the dynamics of this system are fast, so it is crucial to develop a high-performance control techniques that quickly calculate the needed control actions for such a fast system. Developing reliable dynamic models and control techniques for the optimal operation of SCR has attracted the attentions of researchers in academia and industry. The models developed for SCR include a set of coupled parabolic and first-order hyperbolic partial differential equations (PDEs) in combination with several ordinary differential equations (ODEs) that represent the reactions that occur in the solid phase. These equations are nonlinear. Thus SCR is a complex system that may be modelled with coupled nonlinear ODEs and PDEs. It is noteworthy that all of the ODEs and PDEs used in the project have been developed on the basis of mass and energy balances.

To the best of our knowledge, there is not any work on the optimal control of a system consisting of coupled hyperbolic, parabolic PDEs and ODEs. Currently, all controllers designed for the SCR have been based on the discretization of the SCR models into a set of ODEs (i.e., called early lumping) and applying the control algorithms developed for ODEs. One of the big drawbacks of the early lumping is that the ODEs obtained based on the discretization of PDEs may not capture important dynamics of a system, which reduces the effective control performance. Thus, a large number of ODEs may be required in order to obtain the desired control performance, which results in the increase of the required computation. This increased computation can result in an unrealizable closed-loop controller. In this work, an optimal controller based on closed-loop control techniques that belongs to the class of distributed parameter control is proposed. This technique uses a novel numerical method for solving systems modelled with coupled hyperbolic and parabolic PDEs. Among the many different numerical methods developed for solving hyperbolic or parabolic PDE, such as finite difference and finite element methods, we chose to use methods involving the exact transformation of PDEs into ODEs. Here we use the method of characteristics to change hyperbolic PDEs into a set of ODEs that are solved along characteristic curves. In addition, spectral decomposition is used to convert parabolic PDEs into a finite set of ODEs that capture important dynamics of parabolic PDEs. The method of characteristics and spectral decomposition are employed in this work to transform a distributed parameter system into a lumped system. The PDEs that found in the complex models considered in the work are transformed into a finite number of ODEs; then, characteristics-based nonlinear model predictive control (CBNMPC) is used as to control the SCR in diesel-powered vehicles. NMPC belongs to the family of optimal control techniques, and it can be used for controlling complex and nonlinear systems. The type of the control problem that exists in SCR is the boundary control problem. The control objectives in SCR are to reduce the amount of NO_x emissions and the ammonia slip (the NH_3 concentration at tailpipe) as far as possible. In addition, optimal open-loop control approaches using direct transcription (DT) method, are used to determine the best achievable control performance, assuming that future operating conditions and disturbances of plant are known. In addition, a PI controller is designed to investigate how using advanced controllers can improve the control performance of the SCR. Finally, the performances of the all control strategies are compared using several simulation studies.

This work includes several sections. In the second chapter, the SCR and its model are discussed. One-dimensional models for SCR and the proposed numerical solutions of systems with coupled hyperbolic and parabolic PDEs, and a set of ODEs are discussed. In addition, the model used for SCR is validated by some numerical simulations. In the third chapter, CBNMPC, DT and PI controllers are designed for SCR. In the last chapter, the work is summarized and conclusion is discussed. Finally, directions for the future work are proposed.

Chapter 2

Process Description and Modelling of SCR

In this chapter, several topics are covered. First, an overview of the SCR process is given; in addition, the parameters that affect its operation and control performance, and the challenges that exist in the operation of the SCR reactor are discussed. An automotive urea SCR system consists of three subsystems: the urea dosage system, catalyst system and control system. These subsystems are discussed in Section 2.1. Secondly, the reactions that occur in SCR are explained in Section 2.2. Finally, modelling of the SCR is discussed in Section 2.3.

2.1 Process Description

Two different types of SCR exist. The first type uses ammonia or urea solution to reduce nitrogen monoxide (NO) and nitrogen dioxide (NO_2) to nitrogen and water. Urea is favored because it can be handled more easily. The second type uses hydrocarbons to reduce the NO_x emissions. It is convenient to use diesel fuel as the source for the hydrocarbons, but a SCR can use other hydrocarbons. The ammonia-based SCR can reduce up to 95% NO_x emissions; whereas, NO_x reduction by the hydrocarbon injection is limited to approximately 40%. Also, hydrocarbon-based SCR is sensitive to temperature [3].

The two most common designs of SCR catalyst geometry used today are honeycomb and plate. The honeycomb configuration usually is an extruded ceramic coated with a washcoat containing a catalyst. The honeycomb forms are smaller than plate types, which makes honeycomb forms suitable for using in automotive industries; however, they have the disadvantage of higher pressure drops and they can easily get plugged. Plate-type catalysts have the advantage of lower pressure drops than honeycomb forms; in addition, they are less susceptible to plugging and fouling than the honeycomb types. Plate configurations are much larger and more expensive than honeycomb configurations, so the honeycomb configuration is used in cars [7].

SCR systems are sensitive to contamination and plugging stemming from normal operation or abnormal events. The large majority of catalysts are supported on porous structures that give the catalyst a high surface area for the reduction of NO_x emissions. The performance of a SCR can be degraded by poisons, (e.g., halogens, alkaline metals, arsenic, phosphorus, antimony, chrome, copper), which destroy the chemistry of the catalyst and make SCR ineffectual; as a matter of fact, the NO_x reduction decreases, and unwanted oxidation of ammonia increases due to poisons existing in exhaust gas emissions [7, 8].

Factors that influence the performance of SCR include the distribution of ammonia in the gas stream upstream of monolith and gas velocity profile through the catalyst. In addition, the angle of ammonia injection plays an important role in effectively reducing NO_x emissions because it affects the proper distribution of ammonia. Another facet of operation of SCR is the proper determination of ammonia flow for each operating condition. The ammonia flow is in general controlled based on NO_x measurements taken from the gas stream or preexisting performance curves from an engine manufacturer. The ammonia slip is an industry term for unreacted ammonia exiting from SCR. This occurs when more ammonia is injected into gas stream than the amount needed for the NO_x reduction. Temperature is one of the important factors limiting SCR performance. Diesel engines all have a period of start-up during which exhaust temperatures are too low for the ammonia to react with NO_x emissions; as a result, there are NO_x emissions or a large ammonia slip in the tailpipe [3, 7, 8].

Urea solutions are used as a source of ammonia in SCR, but in exhaust aftertreatments that include both DOC and SCR, because of limitations on the residence time between DOC and SCR catalyst and the higher dynamics of system, the complete conversion of urea could not be achieved; therefore, gaseous NH_3 rather than urea solutions is injected after DOC. This situation rarely happens, so passenger cars use urea solutions as the external source of ammonia. The SCR catalysts used in vehicles are typically an extruded monolith with 300 cells per square inch (cpsi), a wall thickness of 0.32 mm with different catalyst volumes such as, 25, 32 and 43 litres.

There are several operating modes in a drive cycle. In other words, the engine speed and load changes during a drive cycle because a driver accelerates, decelerates or stop the vehicle; as a result, the outlet temperature and concentration of the components of diesel emission change. Thus, the inlet condition of SCR constantly changes, so there is no steady state operation in SCR. The control of SCR is therefore a challenging issue. A typical process diagram of SCR is shown in Figure 2.1.

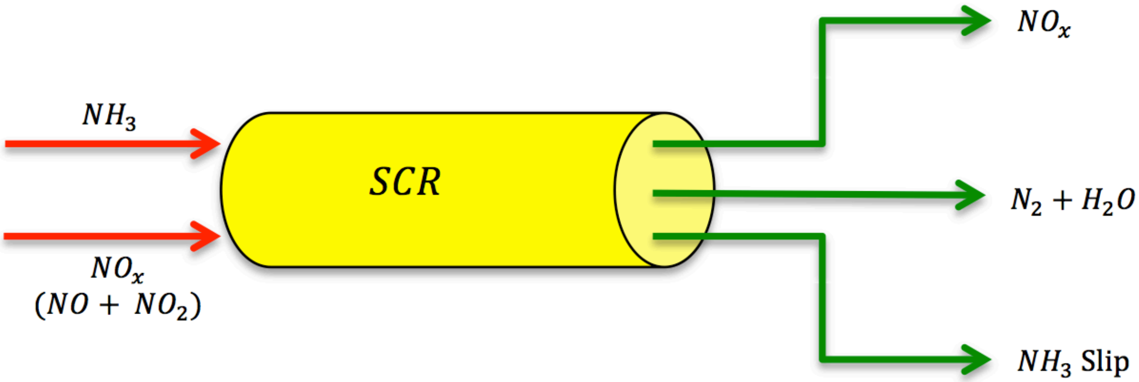

Figure 2.1: Automotive ammonia SCR system layout.

2.1.1 SCR Control Problem

The amount of ammonia adsorbed on the SCR catalyst should be kept as high as possible to have a high NO_x reduction efficiency; however, high ammonia storage can lead to ammonia slip, which is also undesirable. Good control performance is achieved if the tailpipe concentration of NO_x is less than 50 ppm, and the ammonia slip is less than 20 ppm, so the control objective in SCR operation is to minimize the ammonia slip and the NO_x concentration at the outlet of the SCR. The ammonia dosage is the only manipulated variable. The optimal dosage of urea in SCR is the challenging issue in diesel-powered engines. Furthermore, the dynamics of this system are so fast, so it is crucial to develop a high-performance control technique that calculates the control actions for such a fast system. Another challenge is the selection of sampling time in

SCR because it is always chosen shorter than or equal to the residence time of gas emissions flowing through SCR, but there are some factors that must be considered; for example, there are some disturbances that may affect the control performance of a SCR. First of all, the inlet concentration of NO_x continuously fluctuates due to the changes in the speed of diesel engine. Secondly, if the urea solution is used as an external source of ammonia, the under/overdosage of urea solution will be a potential disturbance in the control of SCR. The last disturbance is the inlet temperature of the gas emissions. Thus, it is necessary to take the maximum frequency of the disturbances in SCR into consideration to select a proper sampling time instant. During a drive cycle, the speed of the diesel engine changes, which results in changes of velocity of the gas emissions flowing through the exhaust aftertreatment system. Thus, the variable velocity of the gas emissions is considered to be one of the factors that have a great influence on the sampling time.

A gas hourly space velocity that ranges from 1,000/h to 211,000/h, can be considered for SCR in a driving condition; however, lower gas velocities can be considered in the special conditions like engine start-up. Furthermore, operating temperatures and NO_2/NO_x ratios range from 230 ^oC to 460 ^oC and from 10% to 44%, respectively. Sampling times of around 2 Hz before and after the catalyst systems are usually used to measure both temperatures and emissions with using various types of spectrometers for NO, NO_2 and NH_3 [3]. There is no measurement along SCR, so it is impossible to measure the temperatures and the concentrations of the components along SCR. The measurements of temperatures and concentrations are only available at the inlet and outlet of SCR.

As discussed, the space velocity in SCR may range from 1,000/h to 211,000/h, so it is necessary to design a controller with variable sampling time. Design of a controller with fixed sampling time may reduce the control performance of a system because the residence time of the gas mission flowing through SCR constantly changes; of course, other factors in selecting the sampling time should be considered to have good control performance. Determining a proper sampling period for complex systems is always challenging, so one needs to perform some simulations to determine the proper sampling time for a system.

2.2 Chemistry Model

To form the required reducing reagent for the NO_x reduction in the SCR catalyst, an aqueous urea solution is injected through a nozzle, such that it is atomized in the exhaust pipe. The main steps in the NH_3 formation process are [9]:

$$\mathrm{H_4N_2CO} \longrightarrow \mathrm{NH_3} + \mathrm{HNCO} \tag{2.1}$$

$$\mathrm{HNCO} + \mathrm{H_2O} \longrightarrow \mathrm{NH_3} + \mathrm{CO_2} \tag{2.2}$$

The thermal decomposition reaction (2.1) takes place upstream of the SCR catalyst. The amount of NH_3 formed depends on temperature and space velocity (i.e., the reciprocal of residence time). From measurements in a flow reactor, it has been observed that the contribution of the hydrolysis reaction (2.2) to NH_3 formation upstream of the SCR catalyst is negligible. The hydrolysis reaction needs to be catalyzed and occurs inside the SCR reactor [9].

Using the formed NH_3, the nitrogen oxides emitted by the engine are reduced and converted to harmless products (nitrogen and water) over an SCR catalyst. The reactions are [9]:

$$\mathrm{4NH_3} + \mathrm{2NO} + \mathrm{2NO_2} \longrightarrow \mathrm{4N_2} + \mathrm{6H_2O} \tag{2.3}$$

$$\mathrm{4NH_3} + \mathrm{4NO} + \mathrm{O_2} \longrightarrow \mathrm{N_2} + \mathrm{6H_2O} \tag{2.4}$$

$$\mathrm{8NH_3} + \mathrm{6NO_2} \longrightarrow \mathrm{7N_2} + \mathrm{12H_2O} \tag{2.5}$$

The most desirable pathway is the fast-SCR reaction (2.3), which is considerably faster than the standard SCR reaction (2.4) and reaction (2.5). For high temperatures, maximum achievable NO_x conversion can be limited due to ammonia oxidation. The reaction mechanisms are [9]:

$$\mathrm{4NH_3} + \mathrm{3O_2} \longrightarrow \mathrm{2N_2} + \mathrm{6H_2O} \tag{2.6}$$

$$\mathrm{NH_3} + \mathrm{5O_2} \longrightarrow \mathrm{4NO} + \mathrm{6H_2O} \tag{2.7}$$

2.3 Modelling

A monolith reactor has been used for the simulations of the SCR. In many cases, it can be considered as a single channel. The most important processes in a monolith channel are: convection in the exhaust gas; heat and mass transfer between the flowing gas and the washcoat; internal diffusion within the washcoat; catalytic reactions in the washcoat; heat and mass accumulation; and heat conduction in solid phase.

In the following sections, a one-dimensional (1D) spatial model is used as the common model for SCR; then, a numerical method is developed to solve this 1D spatial model including coupled hyperbolic and parabolic PDEs and several ODEs. This new numerical method transforms the 1D spatial model into a finite set of ODEs.

2.3.1 1-Dimensional Spatial Model

The heterogeneous (1D) plug-flow model of the catalytic monolith channel with surface component deposition [10] has been used for the simulations of the SCR. This model was developed based on the first principles. Despite the drawbacks arising from implicitly including the internal diffusion effects in the reaction kinetics, the 1D plug-flow model is used extensively in automotive industries [3].

The complete model is [3, 11]:

1) the mass balances of the individual components in the flowing gas are shown in Equation(2.8) that belongs to the class of hyperbolic PDE.

$$\frac{\partial c_k^g(z,t)}{\partial t} = -v\frac{\partial c_k^g}{\partial z} + \frac{k_c^k a}{\epsilon^g}(c_k^s - c_k^g), \quad k = NO, NO_2, NH_3, O_2 \tag{2.8}$$

2) the mass balances of the individual components in the washcoat pores are shown in Equations(2.9)-(2.12).

$$\frac{dc_{NO}^s(z,t)}{dt} = \frac{k_c^{NO} a}{1-\epsilon^g}(c_{NO}^g - c_{NO}^s) - \frac{a}{1-\epsilon^g}(0.5R_1 + R_2 - R_5) \tag{2.9}$$

$$\frac{dc_{NO_2}^s(z,t)}{dt} = \frac{k_c^{NO_2} a}{1-\epsilon^g}(c_{NO_2}^g - c_{NO_2}^s) - \frac{a}{1-\epsilon^g}(0.5R_1 + 0.75R_3) \tag{2.10}$$

$$
\begin{aligned}
\frac{dc^s_{NH_3}(z,t)}{dt} &= \frac{k_c^{NH_3}a}{1-\epsilon^g}(c^g_{NH_3}-c^s_{NH_3}) - \frac{a}{1-\epsilon^g}(R_1+R_2+R_3+R_4+R_5) \\
&\quad - \frac{a}{1-\epsilon^g}(R_{ad}-R_{des}) \qquad (2.11)\\
\frac{dc^s_{O_2}(z,t)}{dt} &= \frac{k_c^{O_2}a}{1-\epsilon^g}(c^g_{O_2}-c^s_{O_2}) - \frac{a}{1-\epsilon^g}(\frac{3}{4}R_4+\frac{5}{4}R_5) \qquad (2.12)
\end{aligned}
$$

3) the mass balances of ammonia on the catalyst surface is shown in Equation(2.13). In this work, the mass balance of ammonia on the catalyst surface is only considered.

$$
\frac{d\psi_{NH_3}(z,t)}{dt} = \frac{1}{\Psi^{cap}_{NH_3}}(R_{ad}-R_{des}-aR_4) \qquad (2.13)
$$

4) the total enthalpy balance of the flowing gas is shown in Equation(2.14) that is also a hyperbolic PDE.

$$
\frac{\partial T^g(z,t)}{\partial t} = -v\frac{\partial T^g}{\partial z} + \frac{k_h a}{\rho^g cp^g \epsilon^g}(T^s-T^g) \qquad (2.14)
$$

5) the enthalpy balance of the solid phase is shown in Equation(2.15) that is a parabolic PDE.

$$
\begin{aligned}
\frac{\partial T^s(z,t)}{\partial t} &= \frac{\lambda^s}{\rho^s cp^s}\frac{\partial^2 T^s}{\partial z^2} - \frac{k_h a}{\rho^s cp^s(1-\epsilon^g)}(T^s-T^g) - \frac{k_{ext}a_{ext}}{\rho^s cp^s(1-\epsilon^g)}(T^s-T^{ext}) \\
&\quad - \frac{1}{\rho^s cp^s(1-\epsilon^g)}\sum_{j=1}^{5}\Delta H_j R_j \qquad (2.15)
\end{aligned}
$$

where: c_k is the concentration of component 'k'; v is the linear gas velocity; k_c is the mass transfer coefficient; a is the mass and heat transfer area per unit of catalyst volume; ϵ is the porosity in the catalytic washcoat layer or the percentage of the open frontal area in monolith reactor; ψ is the coverage of stored ammonia on the surface of catalyst; R in which the terms including ψ and c^s appear, is the reaction rate in SCR; Ψ^{cap} is the storage capacity related to the washcoat volume; ρ is the density; c_p is the specific heat capacity; k_h is the heat transfer coefficient; λ is the thermal conductivity; T^{ext} is the temperature of surroundings; and ΔH is the standard reaction enthalpy. The superscripts g and s stand for the gas and solid phase, respectively. In fact, the model of SCR includes hyperbolic and parabolic partial differential equations (PDEs), and some ordinary differential equations (ODEs) that are coupled. These processes are shown in Figure 2.2.

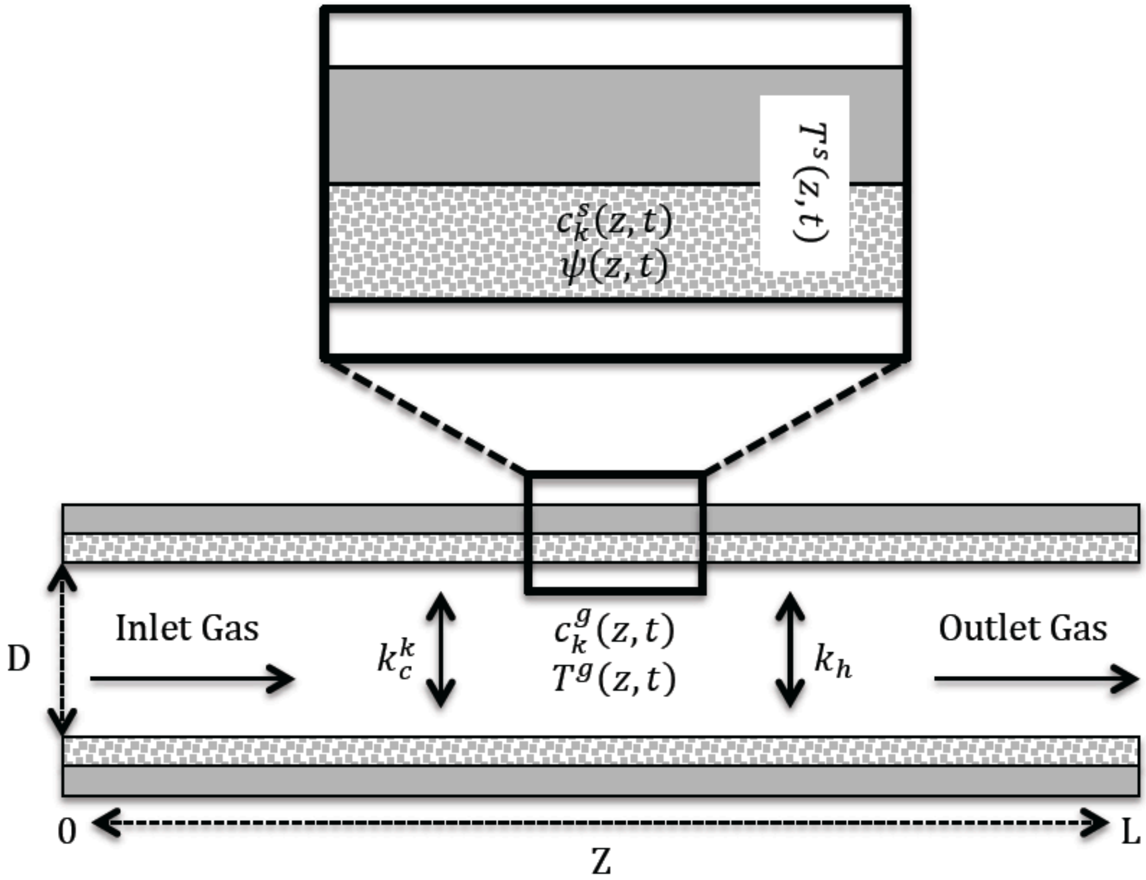

Figure 2.2: Monolith channel and chemical parameters considered in the models.

The following, reasonable assumptions are considered in the SCR model: 1) the ideal gas behavior and constant pressure (i.e., the system is open to the ambient atmosphere, and has a very low pressure drop); 2) the relatively low concentration of key reactants allows approximation of diffusion processes by Fick's law and assuming negligible changes in the number of moles produced by the reactions; 3) the axial dispersion and heat conduction effects in the flowing gas can be neglected; 4) the description of heat and mass transfer between bulk of flowing gas and catalytic washcoat can be approximated by distributed transfer coefficients, calculated from suitable correlations; and 5) the effective heat conductivity, density and heat capacity are used for the entire solid phase, which consists of catalytic washcoat layer and monolith substrate (wall).

The Sherwood and Nusselt numbers were assumed to have the values 4 for the SCR, as this value is extensively used in the monolith reactors [12,13], which is based on the fact that the flow is laminar and most of the reactor has fully developed flow. The hydraulic diameter of channel (D) is 1.5 mm and the length of reactor (L) is 12 cm. The boundary conditions used at the inlet (z=0) and at the outlet (z=L) of the monolith are shown in Equations(2.16)-(2.17). The reaction rates are shown in Equations(2.18)-(2.24). The parameters, mass and heat transfer coefficients, and functions used to express the reaction kinetics that are used in Equations(2.8)-(2.15) are shown in Tables 2.1 and 2.2, respectively.

$$T^g = T^g_{in}, c^g_k = c^g_{k,in}, \quad k = NO, NO_2, NH_3, O_2 \quad at \quad z = 0 \tag{2.16}$$

$$\frac{\partial T^s}{\partial z} = 0, \quad at \quad z = 0, \quad z = L \tag{2.17}$$

$$R_1 = 2.53 * 10^6 e^{\frac{-3007}{T^s}} \frac{c^s_{NO} c^s_{NO_2} c^s_{NH_3}}{1 + 1.2042 * 10^{-3} c^s_{NH_3}} \tag{2.18}$$

$$R_2 = 2.36 * 10^8 e^{\frac{-7151}{T^s}} \frac{c^s_{NO} c^s_{NH_3}}{1 + 1.2042 * 10^{-3} c^s_{NH_3}} \tag{2.19}$$

$$R_3 = 7.56 * 10^8 e^{\frac{-8507}{T^s}} \frac{c^s_{NO_2} c^s_{NH_3}}{1 + 1.2042 * 10^{-3} c^s_{NH_3}} \tag{2.20}$$

$$R_4 = 1.32 * 10^7 e^{\frac{-15034}{T^s}} \psi_{NH_3} \tag{2.21}$$

$$R_5 = 9.11 * 10^{10} e^{\frac{-14503}{T^s}} \frac{c^s_{O_2} c^s_{NH_3}}{(1 + 1.2042 * 10^{-3} c^s_{NH_3})(1 + 1.5053 * 10^{-3} c^s_{O_2})} \tag{2.22}$$

$$R_{ad} = 0.82 c^s_{NH_3} (1 - \psi_{NH_3}) \tag{2.23}$$

$$R_d es = 3.67 * 10^6 e^{\frac{-12992(1 - 0.310\psi_{NH_3})}{T^s}} \psi_{NH_3} \tag{2.24}$$

Table 2.1: Model parameters for SCR [9]

Parameter	Value	Unit
a	2666	$[m^2 m^{-3}]$
a_{ext}	1	$[m^2 m^{-3}]$
k_{ext}	35	$[W m^{-2} K^{-1}]$
ϵ^g	0.68	[%]
ρ^s	1770	$[kg m^{-3}]$
cp^s	900	$[J kg^{-1} K^{-1}]$
λ_s	1	$[W m^{-1} K^{-1}]$
$\psi_{NH_3}^{cap}$	209	$[W m^{-1} K{-1}]$
ΔH_1	-378.534	$[kJ mol^{-1}]$
ΔH_2	-407.129	$[kJ mol^{-1}]$
ΔH_3	-341.664	$[kJ mol^{-1}]$
ΔH_4	-316.839	$[kJ mol^{-1}]$
ΔH_5	-226.549	$[kJ mol^{-1}]$

Table 2.2: Mass and heat transfer coefficients for SCR [9]

Parameter	Equation	Unit
k_h	$= 19 + 0.1748 T^g - 18.318 * 10^{-6} (T^g)^2$	$[W m^{-2} K^{-1}]$
k_c^{NO}	$= 2.745 * 10^{-6} (T^g)^{1.75}$	$[m s^{-1}]$
$k_c^{NO_2}$	$= 2.212 * 10^{-6} (T^g)^{1.75}$	$[m s^{-1}]$
$k_c^{NH_3}$	$= 2.959 * 10^{-6} (T^g)^{1.75}$	$[m s^{-1}]$
$k_c^{O_2}$	$= 2.399 * 10^{-6} (T^g)^{1.75}$	$[m s^{-1}]$

2.3.2 Solution of Coupled Hyperbolic and Parabolic PDEs

A new numerical technique is proposed to deal with systems including coupled hyperbolic and parabolic PDE. The proposed technique combines the advantages of the method of characteristics that is used for predicting the exact values of a hyperbolic PDE along the characteristic curves, and spectral decomposition that is used for order reduction of parabolic PDE. This new technique is a combination of two different algorithms that have not yet been used simultaneously to solve a system.

The method of characteristics, spectral decomposition and combination procedure are explained in detail in the subsequent subsections.

Method of Characteristics

The method of characteristics provides a geometric solution method to the hyperbolic class of the distributed parameter systems by considering characteristics curves [14]. Any given hyperbolic PDE system can be converted into an equivalent system including the differentiation along the defined characteristics. Then, every hyperbolic PDE can be transformed into an ODE along its characteristic curves; therefore, the method of characteristics is deemed to be a powerful method for solving hyperbolic PDEs [15–19]. In this section, the method of characteristics is introduced for quasi-linear first-order PDEs that are used in SCR.

A quasi-linear PDE for the function $\psi(t, z_1, \dots, z_n)$ on the manifold $M \times R \in R^{n+1}$ is shown in Equation(2.25).

$$\frac{\partial \psi}{\partial t} = -\sum_{i=1}^{n} a_{hi}(z_i, \psi, u)\frac{\partial \psi}{\partial z_i} + f_h(z_1, \dots, z_n, \psi, u) \tag{2.25}$$

where: t is the time; $X = [z_1, \dots, z_n]$ is a point in the manifold $M \in R^n$; $a_{hi}(z_i, , u)$ and $f_h(z_1, \dots, z_n, \psi, u)$ are continuous functions; and u are inputs to the system, such as parameters of the system and manipulated variables. Suppose $\psi(t, z_1, \dots, z_n)$ is the solution of Equation(2.25). There is the graph $X = \psi(t, z_1, \dots, z_n)$, which has a normal vector $[-\frac{\partial \psi}{\partial t}, -\frac{\partial \psi}{\partial z_1}, \dots, -\frac{\partial \psi}{\partial z_n}, 1]$. The vector $K(t, z_1, \dots, z_n, \psi, u) = [1, a_{h1}(z_1, \psi, u), \dots, a_{hn}(z_n, \psi, u), f_h(z_1, \dots, z_n, \psi, u)]$ that is tangent to the solution graph at each point, is perpendicular to the normal vector of the graph X. The vector field K is the characteristic vector field of the hyperbolic PDE shown in Equation(2.25). The integral curves of the characteristic vector field are named the characteristics of the quasi-linear equation. Also, the ODEs defined by the vector field K are called the characteristic equations, and the characteristic equations of the quasi-linear shown in Equation(2.25) are defined in Equations(2.26)-(2.28).

$$\dot{t} = 1 \tag{2.26}$$

$$\dot{z} = a_h(z, \psi, u) \tag{2.27}$$

$$\dot{\psi} = f_h(z, \psi, u) \tag{2.28}$$

Spectral Decomposition

Parabolic PDE systems appear in the modelling of transport-reaction processes in finite spatial domains, and they consist of spatial differential operators whose spectrum can be divided into two separate parts. The first part includes a finite number of slow and stable eigenvalues and any existing unstable eigenvalues. In the second part, an infinite number of stable and fast eigenvalues exist. The traditional approach to the control of parabolic PDEs comprises the application of the spatial discretization techniques like Galerkin's method to produce a large number of ODEs that precisely show the dynamics of PDE systems. A potential drawback of this approach is that the number of modes that are required to properly describe the dynamics of the system may be very large; which can increase the complexity of the control design. [14,20–30]

A typical parabolic PDE with the Dirichlet or Neumann boundary conditions is shown in Equation(2.29). The different boundary conditions are shown in Equations(2.30)-(2.31). The eigenvalue problem and its solutions for the operator 'A' described in Equation(2.29), are shown in Equations(2.32)-(2.34).

$$\frac{\partial \chi}{\partial t} = A\chi + f(\chi, t, z, u), \quad A\chi = \alpha \frac{\partial^2 \chi}{\partial z^2}, \quad \chi(z, 0) = \chi_0 \tag{2.29}$$

$$Dirichlet\, Boundary\, Condition: \chi(0, t) = 0, \quad \chi(L, t) = 0 \tag{2.30}$$

$$Neumann\, Boundary\, Condition: \frac{\partial \chi(0, t)}{\partial z} = 0, \quad \frac{\partial \chi(L, t)}{\partial z} = 0 \tag{2.31}$$

$$\alpha \frac{d^2 \phi_j}{dz^2} = \lambda_j \phi_j, \quad j = 1, ..., \infty \tag{2.32}$$

$$for\, Dirichlet\, Boundary\, Condition:$$

$$\lambda_j = -\frac{\alpha (j\pi)^2}{L^2}, \quad \phi_j(z) = \sqrt{\frac{2}{L}} \sin(\frac{j\pi}{L} z), \quad j = 1, ..., \infty \tag{2.33}$$

$$for\,Neumann\,Boundary\,Condition:$$

$$\lambda_0 = 0, \quad \lambda_j = -\frac{\alpha(j\pi)^2}{L^2}, \quad \phi_0 = \frac{1}{\sqrt{L}}, \quad \phi_j(z) = \sqrt{\frac{2}{L}}\cos(\frac{j\pi}{L}z), \quad j = 1, ..., \infty \tag{2.34}$$

where λ_j is the eigenvalue and $\phi_j(z)$ is the relevant eigenfunction of each λ_j. Next, the standard Galerkin's method is applied to the infinite dimensional system of Equation(2.29) to derive a finite-dimensional system. The modal subspaces of 'A', are defined as $H_s = span\{\phi_1, \ldots, \phi_m\}$ and $H_f = span\{\phi_{m+1}, \phi_{m+2}, \ldots\}$. The state χ shown in Equation(2.29) can be decomposed into the fast and slow states by defining the orthogonal projection operators P_s and P_f. Finally, the system defined in Equation(2.29) is transformed into Equations(2.35)-(2.37) with using P_s and P_f.

$$\chi = \chi_s + \chi_f = P_s\chi + P_f\chi \tag{2.35}$$

$$\frac{d\chi_s}{dt} = A_s\chi_s + f_s(\chi_s, \chi_f, t, z, u), \quad \chi_s(z, 0) = P_s\chi_0 \tag{2.36}$$

$$\frac{d\chi_f}{dt} = A_f\chi_f + f_f(\chi_s, \chi_f, t, z, u), \quad \chi_f(z, 0) = P_f\chi_0 \tag{2.37}$$

where: $A_s = P_sA = diag(\lambda_j)$ is a diagonal matrix of dimension $M \times M$; $\beta_s = P_s\beta$; $A_f = P_fA$ is an unbounded differential operator, which is exponentially stable; and $\beta_f = P_f\beta$. The amplitudes of the eigenmodes of the PDE of Equation(2.29) are achieved by using the Galerkin's method; therefore, the high-order ODE system that describes the temporal evolution of the amplitudes of the first h eigenmodes (a_s and a_f) is described in Equations(2.38)-(2.39).

$$\frac{da_s}{dt} = A_sa_s + f_s(a_s, a_f, t, u), \quad \chi_s = \sum_{i=1}^{m} a_i\phi_i \tag{2.38}$$

$$\frac{da_f}{dt} = A_fa_f + f_f(a_s, a_f, t, u), \quad \chi_f = \sum_{i=m+1}^{h} a_i\phi_i \tag{2.39}$$

To develop a lower order model for the system shown in Equation(2.29), the slow eigenmodes of the system are used, and the fast ones are neglected; so, the final ODE system is shown in Equation(2.40). A simple criterion for the selection of the number of slow eigenmodes is that the first fast eigenvalue must be at least 100 times bigger than the smallest eigenvalue of the slow part [14, 20, 24].

$$\frac{da_s}{dt} = A_s a_s + f_s(a_s, 0, t, u), \quad \chi = \chi_s = \sum_{i=1}^{m} a_i \phi_i \tag{2.40}$$

Combination of Method of Characteristics and Spectral Decomposition

To simulate SCR, we require a combined approach to solve Equations(2.26)-(2.28) and (2.40) along predefined characteristic lines. The finite set of ODEs that are solved simultaneously are shown in Equation(2.41)-(2.44).

$$\frac{dz^n}{dt} = a_h(a_s, \psi^n, t, z^n, u), \quad n = 1, ..., K \tag{2.41}$$

$$\frac{d\psi^n}{dt} = f_h(a_s, \psi^n, t, z^n, u), \quad n = 1, ..., K \tag{2.42}$$

$$\frac{da_s}{dt} = A_s a_s + f_s(a_s, \tilde{\psi}, t, u) \tag{2.43}$$

$$\tilde{\psi} = \Psi(\psi^1, ..., \psi^K) \tag{2.44}$$

where: $\tilde{\psi}$ is a function of all ψ^n along the tube; superscript n shows the spatial point or characteristic line along the tube; and the total number of characteristic lines is K. The number of the spatial points affects the accuracy of the projection of states that arise from hyperbolic PDEs; as a result, the accuracy of the numerical simulations is affected.

2.3.3 Validation of SCR Model

To validate the selected model and the numerical technique developed in this work, a simulation study is performed with a scenario that is defined in Table 2.3. The simulation time is divided into 13 operating modes and each operating mode lasts two times of residence time. There are several scenarios in the literature, but the selected scenario is the hardest one to control. In the predefined scenario, the exhaust aftertreatment system is cold when the diesel engine starts to work. The inlet concentration of ammonia is considered zero to perform an open-loop simulation.

Table 2.3: simulation scenario for SCR [9]

Mode	Temperature [^{0}C]	Velocity [m/s]	NO$_x$ [ppm]
1	120	0.069	150
2	303	0.148	749
3	425	0.197	1146
4	493	0.236	1294
5	515	0.318	1250
6	290	0.210	596
7	368	0.282	1045
8	416	0.363	1176
9	470	0.435	1215
10	270	0.262	497
11	334	0.350	778
12	376	0.439	1003
13	439	0.493	1113

Equations(2.9)-(2.15) are transformed into a set of ODEs using the numerical technique developed in this work. The new set of equations used for the simulation and control are shown in Equations(2.45)-(2.56).

$$\frac{dc^g_{k,n}(t)}{dt} = \frac{k^k_{c,n}a}{\epsilon^g}(c^s_{k,n} - c^g_{k,n}), \quad k = NO, NO_2, NH_3, O_2, \quad n = 1,..,N \tag{2.45}$$

$$\frac{dc^s_{NO,n}(t)}{dt} = \frac{k^{NO}_{c,n}a}{1-\epsilon^g}(c^g_{NO,n} - c^s_{NO,n}) - \frac{a}{1-\epsilon^g}(0.5R_{1,n} + R_{2,n} - R_{5,n}), \quad n = 1,..,N \tag{2.46}$$

$$\frac{dc^s_{NO_2,n}(t)}{dt} = \frac{k^{NO_2}_{c,n}a}{1-\epsilon^g}(c^g_{NO_2,n} - c^s_{NO_2,n}) - \frac{a}{1-\epsilon^g}(0.5R_{1,n} + 0.75R_{3,n}), \quad n = 1,..,N \tag{2.47}$$

$$\begin{aligned}\frac{dc^s_{NH_3,n}(t)}{dt} &= \frac{k^{NH_3}_{c,n}a}{1-\epsilon^g}(c^g_{NH_3,n} - c^s_{NH_3,n}) - \frac{a}{1-\epsilon^g}(R_{1,n} + R_{2,n} + R_{3,n} + R_{4,n} + R_{5,n}) \\ &\quad - \frac{a}{1-\epsilon^g}(R_{ad,n} - R_{des,n}), \quad n = 1,..,N\end{aligned} \tag{2.48}$$

$$\frac{dc^s_{O_2,n}(t)}{dt} = \frac{k^{O_2}_{c,n}a}{1-\epsilon^g}(c^g_{O_2,n} - c^s_{O_2,n}) - \frac{a}{1-\epsilon^g}(\frac{3}{4}R_{4,n} + \frac{5}{4}R_{5,n}), \quad n = 1,..,N \tag{2.49}$$

$$\frac{d\psi_{NH_3,n}(t)}{dt} = \frac{1}{\Psi^{cap}_{NH_3}}(R_{ad,n} - R_{des,n} - aR_{4,n}), \quad n = 1,..,N \tag{2.50}$$

$$\frac{dT_n^g(t)}{dt} = \frac{k_{h,n}a}{\rho_n^g cp_n^g \epsilon^g}(\tilde{T}_n^s - T_n^g), \quad n = 1,..,N \tag{2.51}$$

$$\frac{d\alpha_i(t)}{dt} = (\gamma_i - \frac{k_{ext}a_{ext}}{\rho^s cp^s(1-\epsilon^g)})\alpha_i - \int_{z=0}^{z=L} \frac{\tilde{k}_h a}{\rho^s cp^s(1-\epsilon^g)}(T^s - \tilde{T}^g)\beta_i dz$$

$$+ \frac{k_{ext}a_{ext}}{\rho^s cp^s(1-\epsilon^g)} \int_{z=0}^{z=L} T^{ext}\beta_i dz - \frac{1}{\rho^s cp^s(1-\epsilon^g)} \int_{z=0}^{z=L} (\sum_{j=1}^{5} \Delta H_j \tilde{R}_j)\beta_i dz,$$

$$i = 0, ..., M \tag{2.52}$$

$$\tilde{T}^g(z,t) = T_n^g(t), \quad at \quad z = \tilde{z}_n + vt, \quad n = 1,..,N, \quad \tilde{T}^g(0,t) = T_{in}^g, \tag{2.53}$$

$$\tilde{R}_j(z,t) = R_{j,n}(t), \quad at \quad z = \tilde{z}_n + vt, \quad n = 1,..,N, \quad \tilde{R}_j(0,t) = R_{j,in}, \quad j = 1,...,5$$

$$\tilde{k}_h(\tilde{z}_n,t) = k_{h,n}(t), \quad at \quad z = \tilde{z}_n + vt, \quad n = 1,..,N, \quad \tilde{k}_h(0,t) = k_{h,in} \tag{2.54}$$

$$T^s(z,t) = \sum_{i=0}^{M} \alpha_i(t)\beta_i(z), \quad \tilde{T}_n^s(t) = \sum_{i=0}^{M} \alpha_i(t)\beta_i(\tilde{z}_n + vt), \quad n = 1,...,N \tag{2.55}$$

$$\beta_0 = \frac{1}{\sqrt{L}}, \quad \beta_i = \sqrt{\frac{2}{L}}\cos(\frac{i\pi z}{L}), \quad \gamma_0 = 0, \quad \gamma_i = -\frac{\lambda^s}{\rho^s cp^s}(\frac{i\pi}{L})^2, \quad i = 1,...,M \tag{2.56}$$

where: α is the amplitude of eigenmode; γ is the eigenvalue; β is the eigenfunction; $\tilde{T}^g$ is a function of gas temperature along SCR; $\tilde{R}$ is a function of the reaction rates along SCR; $\tilde{k}_h$ is a function of heat transfer coefficients along SCR; $\tilde{z}$ are the spatial points; the subscript 'in' stands for the inlet conditions of SCR; N is the number of spatial points or characteristic lines(n); and M is the number of eigenmodes. The reaction rates $[R_{1,n}, \ldots, R_{5,n}]$ along each characteristic line(n) are shown in Equations(2.57)-(2.63); also, the heat and mass transfer coefficients along each characteristic line(n) are shown in Table 2.4. The other parameters can be find in Section 2.3. The reaction rates and the equations for the boundary of SCR at $z = 0$ are shown in Equation(2.64)-(2.78).

$$R_{1,n} = 2.53 * 10^6 e^{\frac{-3007}{\tilde{T}_n^s}} \frac{c_{NO,n}^s c_{NO_2,n}^s c_{NH_3,n}^s}{1 + 1.2042 * 10^{-3} c_{NH_3,n}^s} \tag{2.57}$$

$$R_{2,n} = 2.36 * 10^8 e^{\frac{-7151}{\tilde{T}_n^s}} \frac{c_{NO,n}^s c_{NH_3,n}^s}{1 + 1.2042 * 10^{-3} c_{NH_3,n}^s} \tag{2.58}$$

$$R_{3,n} = 7.56 * 10^8 e^{\frac{-8507}{\tilde{T}_n^s}} \frac{c^s_{NO_2,n} c^s_{NH_3,n}}{1 + 1.2042 * 10^{-3} c^s_{NH_3,n}} \tag{2.59}$$

$$R_{4,n} = 1.32 * 10^7 e^{\frac{-15034}{\tilde{T}_n^s}} \psi_{NH_3,n} \tag{2.60}$$

$$R_{5,n} = 9.11 * 10^{10} e^{\frac{-14503}{\tilde{T}_n^s}} \frac{c^s_{O_2,n} c^s_{NH_3,n}}{(1 + 1.2042 * 10^{-3} c^s_{NH_3,n})(1 + 1.5053 * 10^{-3} c^s_{O_2,n})} \tag{2.61}$$

$$R_{ad,n} = 0.82 c^s_{NH_3,n}(1 - \psi_{NH_3,n}) \tag{2.62}$$

$$R_{des,n} = 3.67 * 10^6 e^{\frac{-12992(1 - 0.310\psi_{NH_3,n})}{\tilde{T}_n^s}} \psi_{NH_3,n} \tag{2.63}$$

Table 2.4: Mass and heat transfer coefficients in each characteristic line(n) for SCR

Parameter	Equation	Unit
$k_{h,n}$	$= 19 + 0.1748 T_n^g - 18.318 * 10^{-6} (T_n^g)^2$	$[W m^{-2} K^{-1}]$
$k_{c,n}^{NO}$	$= 2.745 * 10^{-6} (T_n^g)^{1.75}$	$[m s^{-1}]$
$k_{c,n}^{NO_2}$	$= 2.212 * 10^{-6} (T_n^g)^{1.75}$	$[m s^{-1}]$
$k_{c,n}^{NH_3}$	$= 2.959 * 10^{-6} (T_n^g)^{1.75}$	$[m s^{-1}]$
$k_{c,n}^{O_2}$	$= 2.399 * 10^{-6} (T_n^g)^{1.75}$	$[m s^{-1}]$

The concentrations of the components that appear in solid phase can be represented by ODEs. The values of the components that exist in the solid phase are unknown at the inlet of SCR, so we need to define equations for the boundary of the SCR. We do not need to define any equations for the boundary when there are only hyperbolic PDEs with the Dirichlet boundary conditions. Equations(2.64)-(2.70) show the governing equations of the boundary of SCR at $z = 0$. These equations are simultaneously solved with Equations(2.45)-(2.56).

$$c_k^g(0,t) = c_{k,in}^g, \quad k = NO, NO_2, O_2, \quad c_{NH_3}^g(0,t) = c_{NH_3,in}^g = u \tag{2.64}$$

$$\frac{dc_{NO}^s(0,t)}{dt} = \frac{dc_{NO,in}^s}{dt} = \frac{k_{c,in}^{NO} a}{1 - \epsilon^g}(c_{NO,in}^g - c_{NO,in}^s) - \frac{a}{1 - \epsilon^g}(0.5R_1 + R_{2,in} - R_{5,in}) \tag{2.65}$$

$$\frac{dc^s_{NO_2}(0,t)}{dt} = \frac{dc^s_{NO_2,in}}{dt} = \frac{k^{NO_2}_{c,in}a}{1-\epsilon^g}(c^g_{NO_2,in} - c^s_{NO_2,in}) - \frac{a}{1-\epsilon^g}(0.5R_{1,in} + 0.75R_{3,in}) \tag{2.66}$$

$$\begin{aligned}\frac{dc^s_{NH_3}(0,t)}{dt} = \frac{dc^s_{NH_3,in}}{dt} &= \frac{k^{NH_3}_{c,in}a}{1-\epsilon^g}(c^g_{NH_3,in} - c^s_{NH_3,in}) - \frac{a}{1-\epsilon^g}(R_{1,in} + R_{2,in} + R_{3,in} \\ &+ R_{4,in} + R_{5,in} + R_{ad,in} - R_{des,in})\end{aligned} \tag{2.67}$$

$$\frac{dc^s_{O_2}(0,t)}{dt} = \frac{dc^s_{O_2,in}}{dt} = \frac{k^{O_2}_{c,in}a}{1-\epsilon^g}(c^g_{O_2,in} - c^s_{O_2,in}) - \frac{a}{1-\epsilon^g}(\frac{3}{4}R_{4,in} + \frac{5}{4}R_{5,in}) \tag{2.68}$$

$$\frac{d\psi_{NH_3}(0,t)}{dt} = \frac{d\psi_{NH_3,in}}{dt} = \frac{1}{\Psi^{cap}_{NH_3}}(R_{ad,in} - R_{des,in} - aR_{4,in}) \tag{2.69}$$

$$T^g(0,t) = T^g_{in} \tag{2.70}$$

where u is the manipulated variable (i.e., inlet concentration of ammonia); and subscript 'in' stands for the inputs of SCR. The reaction rates $[R_{1,in}, \cdots, R_{5,in}]$ in the boundary of SCR are shown in Equations(2.71)-(2.78). The heat and mass transfer coefficients in the boundary of SCR can be calculated as given in Table 2.4, which subscript 'n' gets replaced by 'in'.

$$R_{1,in} = 2.53 * 10^6 e^{\frac{-3007}{\tilde{T}^s_{in}}} \frac{c^s_{NO,in}c^s_{NO_2,in}c^s_{NH_3,in}}{1 + 1.2042 * 10^{-3}c^s_{NH_3,in}} \tag{2.71}$$

$$R_{2,in} = 2.36 * 10^8 e^{\frac{-7151}{\tilde{T}^s_{in}}} \frac{c^s_{NO,in}c^s_{NH_3,in}}{1 + 1.2042 * 10^{-3}c^s_{NH_3,in}} \tag{2.72}$$

$$R_{3,in} = 7.56 * 10^8 e^{\frac{-8507}{\tilde{T}^s_{in}}} \frac{c^s_{NO_2,in}c^s_{NH_3,in}}{1 + 1.2042 * 10^{-3}c^s_{NH_3,in}} \tag{2.73}$$

$$R_{4,in} = 1.32 * 10^7 e^{\frac{-15034}{\tilde{T}^s_{in}}} \psi_{NH_3,in} \tag{2.74}$$

$$R_{5,in} = 9.11 * 10^{10} e^{\frac{-14503}{\tilde{T}^s_{in}}} \frac{c^s_{O_2,in}c^s_{NH_3,in}}{(1 + 1.2042 * 10^{-3}c^s_{NH_3,in})(1 + 1.5053 * 10^{-3}c^s_{O_2,in})} \tag{2.75}$$

$$R_{ad,in} = 0.82c^s_{NH_3,in}(1 - \psi_{NH_3,in}) \tag{2.76}$$

$$R_{des,in} = 3.67 * 10^6 e^{\dfrac{-12992(1-0.310\psi_{NH_3,in})}{\tilde{T}^s_{in}}} \psi_{NH_3,in} \tag{2.77}$$

$$\tilde{T}^s_{in} = \sum_{i=0}^{M} \alpha_i(t)\beta(0) \tag{2.78}$$

Equations(2.45)-(2.56) are used for the simulations with 100 modes and 180 spatial points to ensure that all SCR dynamics are captured. These numbers were obtained via numerical simulation. Note that, increasing the numbers of modes and spatial points beyond 100 modes and 180 spatial points, dose not significantly improve the simulation results. The number of spatial points affects the accuracy of the calculation of the integral terms. As a result, it has an influence on the control performance of SCR, so we must carefully pay attention to the selection of the number of spatial points.

Open-Loop Simulation Result

Figure 2.3 shows the 3-dimensional profiles of gas and solid temperatures along SCR. As can be seen, the cold solid consumes the energy of gas phase at the beginning of the SCR. As a result, the temperature of the gas phase decreases sharply, and the temperature of the solid phase increases drastically at the entrance to the SCR. The obtained results are consistent with what is observed in lab-scale SCRs. The NO and NO_2 concentrations are depicted in Figure 2.4. As can be seen, in absence of ammonia injection, the concentration of NO and NO_2 do not decrease and a large amount of NO_x emission emitted into atmosphere.

Thus, the simulation results are consistent with the literature [3, 5–8].

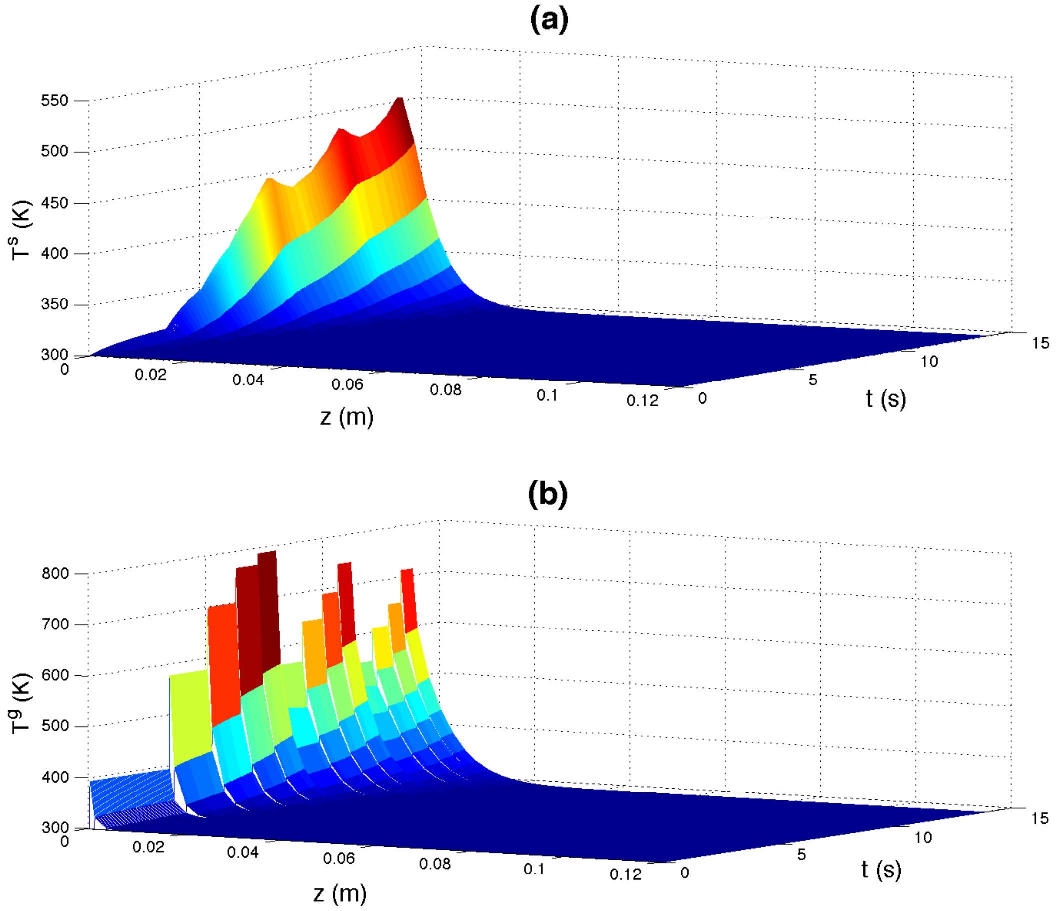

Figure 2.3: Three-dimensional profiles of gas and solid temperatures for open-loop simulation: (a) profile of solid temperature; (b) profile of gas temperature.

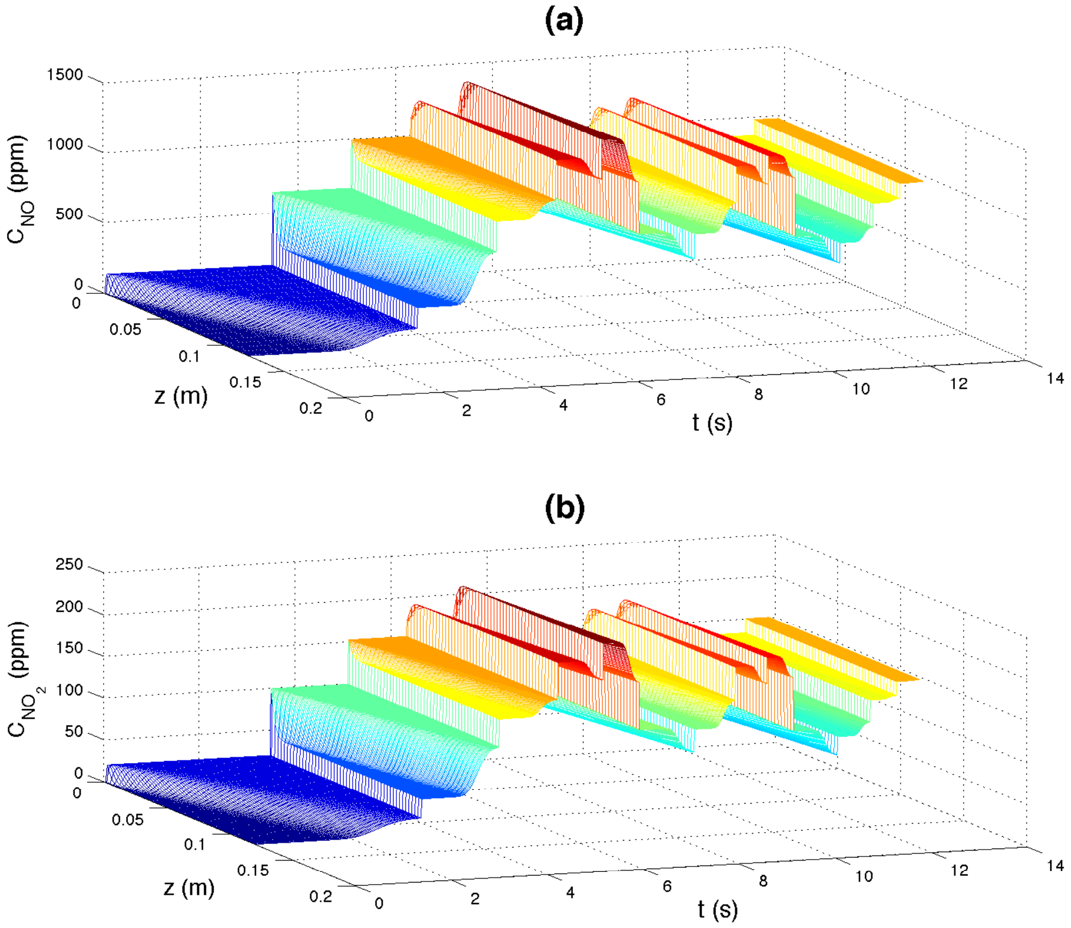

Figure 2.4: Three-dimensional profiles of component concentrations for open-loop simulation: (a) profile of NO; (b) profile of NO_2.

Chapter 3

SCR Control

In this chapter, the control of a system which is described using hyperbolic and parabolic PDEs, and a set of ODEs that are coupled with each other, is discussed. This type of problems is important because it appears in models that exist in the process industries, and in automotive exhaust aftertreatment components like SCR in diesel-powered vehicles.

There exist two feedback approaches to SCR control. One approach is closed-loop NH_3 control, which is attractive because maximum NO_x conversion is the control objective under a given NH_3 slip constraint. This SCR control strategy combines two control modes. The first mode is NH_3 surface coverage control using a 1-D SCR model. The averaged value of the NH_3 surface coverage over the SCR is compared to a reference value of the NH_3 surface coverage. This reference value is the maximum allowable NH_3 storage during a worst-case temperature rise. The second mode is NH_3 slip feedback control. NH_3 slip information is used to directly adjust the urea injection to drive the NH_3 slip toward a given reference concentration level. The NH_3 surface coverage is estimated using an observer.

Another approach is NO_x sensor based strategy that is comprised of a feedforward element that adjusts urea injection on the basis of an engine-out NO_x signal, a nominal stoichiometric ratio (NSR) map, and a dynamic NH_3 desorption compensation. The dosing signal is corrected using feedback information from the post-SCR NO_x sensor. By applying a pulsating urea flow, the amplitudes of the NO_x concentration signal are observed. If the pulses are too high, the algorithm increases the urea injection. If they are too small, NH_3 slip is likely and the algorithm reduces the nominal urea injection. Alternative strategies can be found in the literature [31–33].

To balance high NO_x reduction efficiency and low ammonia slip, several urea dosing control approaches have been recently proposed [9,31–36]. Chen and Tan proposed a 3D dynamic model based on the Navier-Stokes equations for the SCR [37]. They estimated the kinetic parameters of the model using experimental data and an optimization technique that integrates the Taguchi method, a genetic algorithm, and a neural network based auxiliary model. Their results indicate that the optimized SCR can achieve NO_x reduction rate up to 99.93%. In addition, the optimal operating temperature is considerably lower and the ammonia slip is insignificant. They demonstrated that the proposed design provides much better energy savings and is environment-friendly in comparison with the conventional designs [37].

Map-based urea dosage strategies are currently used in vehicles [38]. The Euro-IV and Euro-V emission standards can be achieved by these strategies. To improve catalyst temperature prediction and the engine-out NO_x prediction [39], simple models, which can be considered as the preliminary models of the SCR catalyst dynamics, are used. The need for high NO_x reduction and the introduction of Zeolite catalysts has persuaded researchers to focus on the NH_3 surface coverage control [38]. A reduced order model, obtained on the basis of the first principles for NH_3 surface coverage, can improve NH_3 slip control. Due to safety margins and robustness issues, feedback SCR control has attracted considerable attention. Most of the feedback strategies use a PI controller, a surface coverage observer, and a state feedback controller. Other control approaches are found, such as model reference adaptive control [9], sliding mode control [40], backstepping based nonlinear ammonia surface coverage ratio control [31–33], a computationally-efficient model predictive control assisted method [41] and LPV (linear parameter-varying) gain-scheduled control using robust control techniques and LMIs [42].

All techniques developed to date use models comprised of ODEs to control the SCR and use inlet and outlet sensors for the state and parameter estimation. Measured components are usually NO_x (NO and NO_2) and NH_3. The main drawback of these techniques is that models developed based on ODE cannot capture important SCR dynamics, so the highest performance of the SCR cannot be achieved; however, good performance can be achieved by using models involving a large number of ODEs at the expense of computational time. Using distributed parameter control techniques, one can obtain high level of performance, as the main dynamics of system are captured.

As discussed, all control techniques developed or used to control the SCR have been based on ODEs. A crucial problem of these early lumping techniques or developing models based on ODEs for the systems that are naturally governed by PDEs is that ODE-based models may not capture important system dynamics. This can result in unsatisfactory control performance. Therefore, high performance control design should employ the full complex SCR model rather than an approximation. There exist various control techniques that have been developed to control hyperbolic or parabolic PDEs, but no techniques for systems that include coupled hyperbolic and parabolic PDEs exist in the literature to the best of our knowledge.

Researchers have developed various control techniques for distributed parameter systems, such as optimal control [43–45] and backstepping [46–48]. A control design technique is proposed in this thesis for systems modelled by coupled hyperbolic and parabolic PDEs. The proposed control technique uses a new numerical technique that combines the method of characteristics and spectral decomposition to solve complex systems like the SCR, and is named characteristics-based nonlinear model predictive control (CBNMPC). Characteristics-based model predictive control (CBMPC) was first developed by Shang [15] for systems with linear and quasilinear hyperbolic PDEs. In this work, the CBMPC idea was adapted for control of systems with coupled hyperbolic and parabolic PDEs. CBNMPC uses nonlinear optimization techniques and continuous models rather than using convex optimization techniques for discrete linear or linearized models, as does CBMPC developed by Shang [15].

In addition to the proposed control design technique, an open-loop optimization approach is used to obtain a control performance bench mark for the SCR. The approach uses Direct transcription (DT), which is an optimization technique that can be used to calculate control actions for systems modelled by various types of PDEs.

The optimization-based and CBNMPC techniques are described in Sections 3.1 and 3.2, respectively. Finally, the control approaches are applied to a SCR model in Section 3.3.

3.1 Solution of Dynamic Optimization Problems (DT)

This is an open-loop control technique and can be used to obtain the best control performance possible for a system, assuming that all future operating conditions and disturbances of the system are known. The basic concept of the direct transcription is to discretize a system into the finite set of algebraic equations [49]. This technique transforms the problem into an algebraic optimization problem. There are different methods to discretize a PDE. In this work, orthogonal collocation technique is used. The important property of orthogonal polynomials, such as the Lagrange, Jacobi and Chebyshev polynomials, is that they are orthogonal to each other; therefore, a small number of collocation points are required to achieve an accurate solution [50, 51]. Lagrange polynomials are used to transform the SCR model comprised of hyperbolic and parabolic PDEs and some ODEs, into a set of algebraic equations. In numerical analysis, Lagrange polynomials are used for polynomial interpolation. For a given set of distinct points x_i and numbers y_i, the Lagrange polynomial is the polynomial of the least degree that at each point x_i, the function has the corresponding value y_i. The length and time are normalized between '0' and '1' in order to use orthogonal polynomials. The temporal and spatial points can be selected as roots of orthogonal polynomials.

The temporal and spatial points are considered the roots of the Chebyshev polynomials of the first kind in this work. Chebyshev polynomials are polynomials with the largest possible leading coefficient, but they have the maximum absolute value of 1. Chebyshev polynomials are important in approximation theory because the roots of the Chebyshev polynomials of the first kind, which are also called Chebyshev nodes, are used as nodes in polynomial interpolation. Chebyshev polynomial of the first kind of degree $n \geq 0$ is defined in Equation(3.1). [52–55]

$$T_n(x) = \cos(n \arccos(x)), \quad x \in [-1, 1] \tag{3.1}$$

where $T_n(x)$ is the Chebyshev polynomial of the first kind of degree 'n'. The roots of the Chebyshev polynomials of the first kind of degree 'n' are calculate by Equation(3.2). [52, 55]

$$\bar{x}_k = \cos(\frac{2k-1}{2n}\pi), \quad k = 1, ..., n \tag{3.2}$$

where $\bar{x}_k$ is the roots of the Chebyshev polynomials of the first kind. The roots of the the Chebyshev polynomials of the first kind can be extended to the interval $\tilde{x} \in [a, b]$ using the transformation shown in Equation(3.3). [52, 55]

$$\tilde{x}_k = \frac{1}{2}[(b-a)\bar{x}_k + (a+b)] \quad k = 1, ..., n \tag{3.3}$$

where $\tilde{x}_k$ is the transformed roots of the Chebyshev polynomials of the first kind. In this work, 'a' and 'b' were selected to be '0' and '1', respectively. In fact, the system was normalized between '0' and '1'.

Consider Equation(2.25), which was defined in Section 2.3.2 with the derivative with respect to length in one direction. This equation is discretized into a set of algebraic Equations(3.4)-(3.13) by applying the orthogonal collocation on 'N' and 'M' finite elements within the spatial and temporal domains, respectively.

$$\sum_{j=1}^{M} \bar{\psi}_{pj} \frac{d\bar{\theta}_{jq}}{d\hat{t}} = \tau \left(-\frac{1}{L} \sum_{i=1}^{N} \bar{\psi}_{iq} a_h(\hat{z}, \bar{\psi}_{pq}, \bar{u}_{pq}) \frac{d\bar{\varphi}_{ip}}{d\hat{z}} + f_h(\hat{z}, \bar{\psi}_{pq}, \bar{u}_{pq}) \right), \quad p = 2, .., N, \quad q = 2, ..., M \tag{3.4}$$

$$\hat{z} = \frac{z}{L}, \quad \hat{t} = \frac{t}{\tau} \tag{3.5}$$

$$\psi(\hat{z}, \hat{t}) = \sum_{i=1}^{N} \sum_{j=1}^{M} \bar{\psi}_{ij} \varphi_i(\hat{z}) \theta_j(\hat{t}) \tag{3.6}$$

$$u(\hat{z}, \hat{t}) = \sum_{i=1}^{N} \sum_{j=1}^{M} \bar{u}_{ij} \varphi_i(\hat{z}) \theta_j(\hat{t}) \tag{3.7}$$

$$\varphi_i(\hat{z}) = \prod_{l=1, l \neq i}^{N} \frac{\hat{z} - \hat{z}_l}{\hat{z}_i - \hat{z}_l}, \quad \bar{\varphi}_{ip}(\hat{z}) = \varphi_i(\hat{z}_p) \tag{3.8}$$

$$\theta_j(\hat{t}) = \prod_{l=1, l \neq j}^{M} \frac{\hat{t} - \hat{t}_l}{\hat{t}_j - \hat{z}_l}, \quad \bar{\theta}_{jq}(\hat{t}) = \theta_j(\hat{t}_q) \tag{3.9}$$

$$Boundary\, Conditions : (\hat{z} = 0)$$

$$\bar{\psi}_{1q} = \psi_{in}, \quad q = 2, ..., M \tag{3.10}$$

$$\bar{u}_{1q} = \bar{u}_{1q}, \quad q = 2, ..., M \tag{3.11}$$

$$\mathit{Initial\,Conditions} : (\hat{t} = 0)$$

$$\bar{\psi}_{p1} = \psi_{initial}, \quad p = 1, ..., N \tag{3.12}$$

$$\bar{u}_{p1} = \bar{u}_{initial}, \quad p = 1, ..., N \tag{3.13}$$

where: φ and θ are the Lagrange polynomials; $\bar{\psi}$ and $\bar{u}$ are the coefficients of the Lagrange polynomials; τ is the total time that is simulated, M is the number of temporal points; N is the number of spatial points; and L is the length of the tube.

Also, consider Equation(2.29) defined in Section (2.3.2) with the Neumann boundary condition. The same procedure is applied to this parabolic PDE. The transformed parabolic PDE is shown in Equations(3.14)-(3.22).

$$\sum_{j=1}^{M} \bar{\chi}_{pj} \frac{d\bar{\theta}_{jq}}{d\hat{t}} = \tau \left(\frac{\alpha}{L^2} \sum_{i=1}^{N} \bar{\chi}_{iq} \frac{d^2 \bar{\varphi}_{ip}}{d\hat{z}^2} + f(\bar{\chi}_{pq}, \hat{t}, \hat{z}, \bar{u}_{pq}) \right),$$

$$p = 2, .., N-1, \quad q = 2, ..., M \tag{3.14}$$

$$\chi(\hat{z}, \hat{t}) = \sum_{i=1}^{N} \sum_{j=1}^{M} \bar{\chi}_{ij} \varphi_i(\hat{z}) \theta_j(\hat{t}) \tag{3.15}$$

$$u(\hat{z}, \hat{t}) = \sum_{i=1}^{N} \sum_{j=1}^{M} \bar{u}_{ij} \varphi_i(\hat{z}) \theta_j(\hat{t}) \tag{3.16}$$

$$\mathit{Boundary\,Condition} :$$

$$(\hat{z} = 0)$$

$$\sum_{i=1}^{N} \bar{\chi}_{iq} \frac{d\bar{\varphi}_{i1}}{d\hat{z}} = 0, \quad q = 2, ..., M \tag{3.17}$$

$$\bar{u}_{1q} = \bar{u}_{1q}, \quad q = 2, ..., M \tag{3.18}$$

$$(\hat{z} = 1)$$

$$\sum_{i=1}^{N} \bar{\chi}_{iq} \frac{d\bar{\varphi}_{iN}}{d\hat{z}} = 0, \quad q = 2, ..., M \tag{3.19}$$

$$\bar{u}_{Nq} = \bar{u}_{Nq}, \quad q = 2, ..., M \tag{3.20}$$

$$\mathit{Initial\,Condition} : (\hat{t} = 0)$$

$$\bar{\chi}_{p1} = \chi_{initial}, \quad p = 1, ..., N \tag{3.21}$$

$$\bar{u}_{p1} = \bar{u}_{initial}, \quad p = 1, ..., N \tag{3.22}$$

where $\bar{\chi}$ is the coefficient of the Lagrange polynomials.

3.1.1 Case Study

In this small-scale case study a non-isothermal catalytic packed-bed reactor in which a reaction of the form $A \longrightarrow B$ takes place on a catalyst [24]. The reaction is endothermic and a jacket is used to heat the reactor. Some assumptions are made in modelling of the reactor, such as: negligible diffusion of the gas phase; constant density and heat capacity of the catalyst and the gas; and an excess of species 'A' in the reactor. The resulting dimensionless dynamic model of the process consists of the following set of energy balances: [24]

$$\epsilon \frac{\partial T^g(z,t)}{\partial t} = -\frac{\partial T^g}{\partial z} + h^g(T^c - T^g) - h^g_u(T^g - u) \tag{3.23}$$

$$Boundary\,Condition : T^g(0,t) = 0 \tag{3.24}$$

$$Initial\,Condition : T^g(z,0) = 0 \tag{3.25}$$

$$\frac{\partial T^c(z,t)}{\partial t} = \frac{\partial^2 T^c}{\partial z^2} + Be^{\frac{\gamma T^c}{1+T^c}} - h^c(T^c - T^g) - h^c_u(T^c - u) \tag{3.26}$$

$$Boundary\,Condition : \frac{\partial T^c(0,t)}{\partial z} = \frac{\partial T^c(1,t)}{\partial z} = 0 \tag{3.27}$$

$$Initial\,Condition : T^c(z,0) = 0 \tag{3.28}$$

where: T is the dimensionless temperature; u is the jacket temperature; h is the dimensionless heat transfer coefficient between gas and catalyst; h_u is the heat transfer coefficient between gas/catalyst and jacket temperature; γ is the dimensionless activation energy and B is the dimensionless frequency factor. The superscripts 'g' and 'c' stand for gas and catalyst, respectively. The reactor parameters are shown in Table 3.1.

The main feature of this system is that the heat capacity of the catalytic phase is larger than the heat capacity of the gas phase. Thus, the system has a two-time-scale property. The dynamics of the gas phase are faster than the dynamics of the catalyst phase. The control problem is to enforce a constant catalyst temperature. Since, T^c essentially determines the dynamics of the process, it was selected as the control variable. Then, by manipulating the jacket temperature (u), a desired degree

Table 3.1: Model parameters for catalytic packed-bed reactor [24]

Parameter	Value
ϵ	0.01
γ	21.14
B	-0.03sin(t)
h^g	0.5
h^g_u	0.5
h^c	1.0
h^c_u	15.62

of reaction rate is maintained. The performance index of the open-loop control is shown in Equation(3.29).

$$\min_{u(t)} I = \int_0^{1.3} \int_0^1 [(T^c - r)Q(T^c - r) + uRu]dtdz \tag{3.29}$$

where r is the set point. Manipulated variable forces the catalyst temperature to track a optimal temperature profile over a given period of time.

The algebraic equations obtained from the transformation of Equations(3.23)-(3.28) are shown in Equations(3.30)-(3.40).

$$\epsilon \sum_{j=1}^{M} \bar{T}^g_{pj} \frac{d\bar{\theta}_{jq}}{d\hat{t}} = 1.3 \left(- \sum_{i=1}^{N} \bar{T}^g_{iq} \frac{d\bar{\varphi}_{ip}}{d\hat{z}} + h^g(\bar{T}^c_{pq} - \bar{T}^g_{pq}) - h^g_u(\bar{T}^g_{pq} - \bar{u}_q) \right)$$
$$p = 2, .., N, \quad q = 2, ..., M \tag{3.30}$$

$$\sum_{j=1}^{M} \bar{T}^c_{pj} \frac{d\bar{\theta}_{jq}}{d\hat{t}} = 1.3 \Bigg(\sum_{i=1}^{N} \bar{T}^c_{iq} \frac{d^2\bar{\varphi}_{ip}}{d\hat{z}^2} - 0.03\sin(q) e^{\frac{\gamma \bar{T}^c_{pq}}{1+\bar{T}^c_{pq}}} - h^c(\bar{T}^c_{pq} - \bar{T}^g_{pq})$$
$$- h^c_u(\bar{T}^c_{pq} - \bar{u}_q) \Bigg), \quad p = 2, .., N-1, \quad q = 2, ..., M \tag{3.31}$$

$$T^g(\hat{z}, \hat{t}) = \sum_{i=1}^{N} \sum_{j=1}^{M} \bar{T}^g_{ij} \varphi_i(\hat{z}) \theta_j(\hat{t}) \tag{3.32}$$

$$T^c(\hat{z},\hat{t}) = \sum_{i=1}^{N}\sum_{j=1}^{M} \bar{T}^{c}_{ij}\varphi_i(\hat{z})\theta_j(\hat{t}) \tag{3.33}$$

$$u(\hat{t}) = \sum_{j=1}^{M} \bar{u}_j\theta_j(\hat{t}) \tag{3.34}$$

$$Boundary\, Conditions :$$

$$(\hat{z} = 0)$$

$$\bar{T}^{g}_{1q} = 0, \quad q = 2, ..., M \tag{3.35}$$

$$\sum_{i=1}^{N} \bar{T}^{c}_{iq}\frac{d\bar{\varphi}_{i1}}{d\hat{z}} = 0, \quad q = 2, ..., M \tag{3.36}$$

$$(\hat{z} = 0)$$

$$\sum_{i=1}^{N} \bar{T}^{c}_{iq}\frac{d\bar{\varphi}_{iN}}{d\hat{z}} = 0, \quad q = 2, ..., M \tag{3.37}$$

$$Initial\, Condition : (\hat{t} = 0)$$

$$\bar{T}^{g}_{p1} = 0, \quad p = 1, ..., N \tag{3.38}$$

$$\bar{T}^{c}_{p1} = 0, \quad p = 1, ..., N \tag{3.39}$$

$$\bar{u}_1 = 0.02 \tag{3.40}$$

where $\bar{T}^g$, $\bar{T}^c$ and $\bar{u}$ are expressed in terms of Lagrange polynomials. Also, the spatial and temporal points are roots of the Chebyshev polynomial. M and N were selected to be 22 because as beyond this value simulation results change negligibly.

The performance index defined in Equation(3.29) is transformed into Equation(3.41). The control actions are calculated by solving the optimization problem shown in Equations(3.41)-(3.45). This optimization problem is solved using the function $\backslash fmincon'$ of **MATLAB**, and the Newton-Raphson method is used to solve algebraic Equations(3.30)-(3.39).

$$\min_{\tilde{u}} I = \int_0^1 \int_0^1 [(\tilde{T}^c - r)'Q(\tilde{T}^c - r) + \tilde{u}R\tilde{u}]d\hat{t}d\hat{z} \tag{3.41}$$

$$\tilde{T}^c(p,q) = \bar{T}^c_{pq}, \quad p = 1,..,N, \quad q = 1,...,M \tag{3.42}$$

$$\tilde{u}(q) = \bar{u}_q, \quad q = 2,...,M \tag{3.43}$$

$$subject\, to:$$

$$Eqs.\,(3.30) - (3.40) \tag{3.44}$$

$$0 \leq \bar{u}_q \leq 0.068, \quad q = 2,...,M \tag{3.45}$$

where $\tilde{T}^c$ is a function of the spatial and temporal points for the catalyst temperature; $\tilde{u}$ is a function of the temporal points for the manipulated variable; and the values of Q and R are 1 and 0.001, respectively. The calculated control actions were applied to Equations(3.64)-(3.69) with 5 modes and 20 spatial points. This is assumed to represent the plant for simulation and control evaluation purpose. The details of the numerical simulation of the catalytic packed-bed reactor will be explained in Section 3.2. The results obtained by DT method are depicted in Figures 3.1-3.3.

$$I = \int_0^{1.3} \int_0^1 [(T^c - r)'Q(T^c - r)]dtdz \tag{3.46}$$

As can be seen in Figure 3.1, the jacket temperature increased in order to drive the catalyst temperature to the setpoint 0.05. After 0.4 seconds the setpoint decreased to 0.03, so the jacket temperature decreased to cool the catalyst. Finally, the setpoint increased to 0.06 at time 0.08, and the jacket temperature increased and touched the upper bound until the end of simulation. As can be seen in Figure 3.2, DT perfectly forced the catalyst temperature to its set point (0.05). After 0.4 second, the set point changed to 0.03 and DT drove the catalyst temperature to the new set point. Finally, the set point increased to 0.06 at time 0.8 second, and DT again did its job perfectly. Figure 3.3 shows that the trend of the gas temperature is similar to that of the catalyst temperature. The value of the objective function defined in Equation(3.46) that shows the control performance of controllers, is obtained 0.4427 by DT.

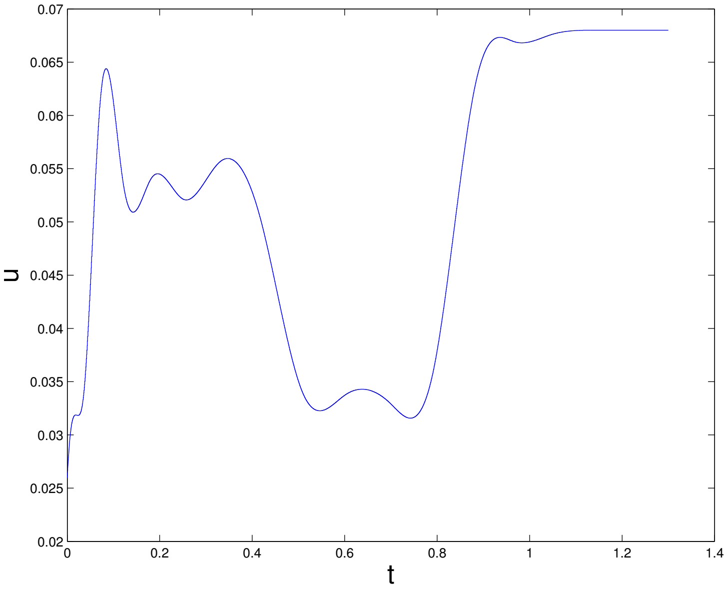

Figure 3.1: Dimensionless control action of catalytic packed-bed reactor with open-loop control technique.

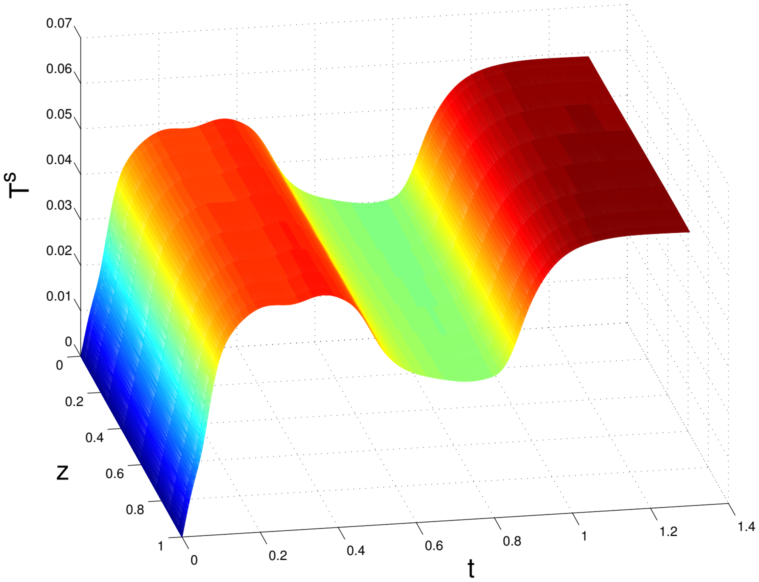

Figure 3.2: Dimensionless catalyst temperature of catalytic packed-bed reactor with open-loop control technique.

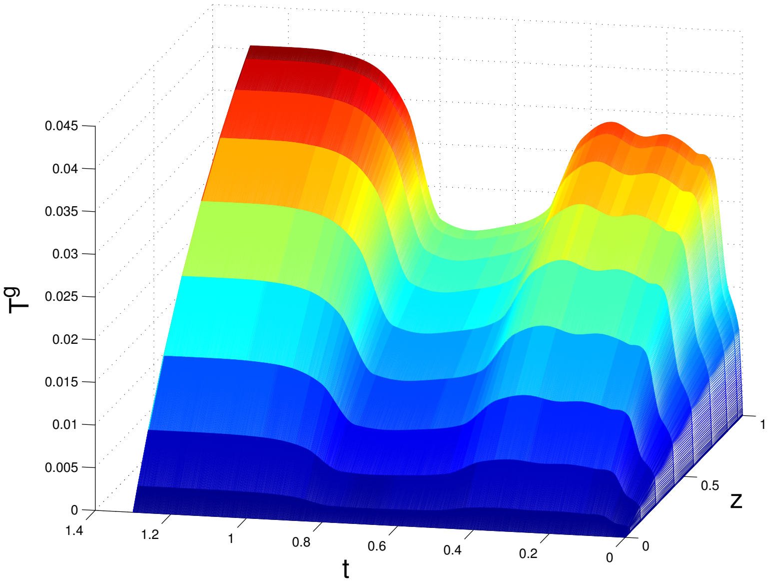

Figure 3.3: Dimensionless gas temperature of catalytic packed-bed reactor with open-loop control technique.

3.2 Closed-Loop Control Technique (CBNMPC)

The closed-loop control approach uses the proposed numerical technique developed in Chapter 2 and NMPC to control systems described by hyperbolic and parabolic PDEs. The proposed control procedure combines the advantages of the method of characteristics, which is used for predicting the exact values of hyperbolic PDEs along the characteristic curves, and spectral decomposition, which is used for order reduction of parabolic PDEs. The proposed closed-loop technique is a combination of three different algorithms that have not yet been used simultaneously to control a system. A small-scale case study is used for the demonstration of this control technique.

One of the main challenges of this type of system is that the hyperbolic and parabolic PDEs are coupled. Furthermore, the system involves several PDEs. Another challenge is that ODEs obtained with the transformation of PDEs are highly nonlinear, which can result in a nonconvex optimal control.

To implement CBNMPC, the starting point of each characteristic curve must be measured as well as the outlet of the tube. In practice, it is not possible to have measurements along a tube, so an observer is needed to estimate the states along a tube. For example, points x_1 and ‘$1'$ in Figure 3.4 are measured, but points $x_2, \ldots, x_m$ are usually hard to measure, so their values can be calculated by an observer; however, the observability of the system must be checked.

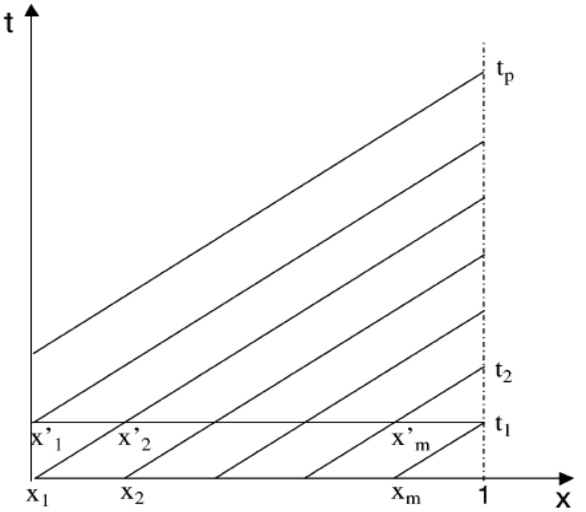

Figure 3.4: Typical characteristic lines for a tube.

The design of CBNMPC for a boundary control problem has not yet been addressed in any work. Figure 3.5 shows typical characteristic lines for a boundary control problem. It is supposed that a tube with length of ‘L' is discretized into 5 points $x_1, \ldots, x_5$. The letters ‘p', ‘m' and ‘r' stand for prediction horizon, control horizon and residence time, respectively. As can be seen in Figure 3.5(a), the control actions are applied to the inlet of the tube, so they can affect the outputs after a residence time. Therefore, the characteristic lines drawn from the inlet to the outlet of the tube are useful in calculating the control actions, and other characteristic lines along which previously applied control actions propagate, are used for numerical purposes [14]. For example, if there is a parabolic PDE that is solved simultaneously with a hyperbolic PDE, the characteristic lines along which previously applied control actions propagate, will be used to solve the whole system. As can be seen in Figure 3.5(b), An effective prediction horizon can be defined from ‘tr' to ‘tp' that must be longer than or equal to the residence time.

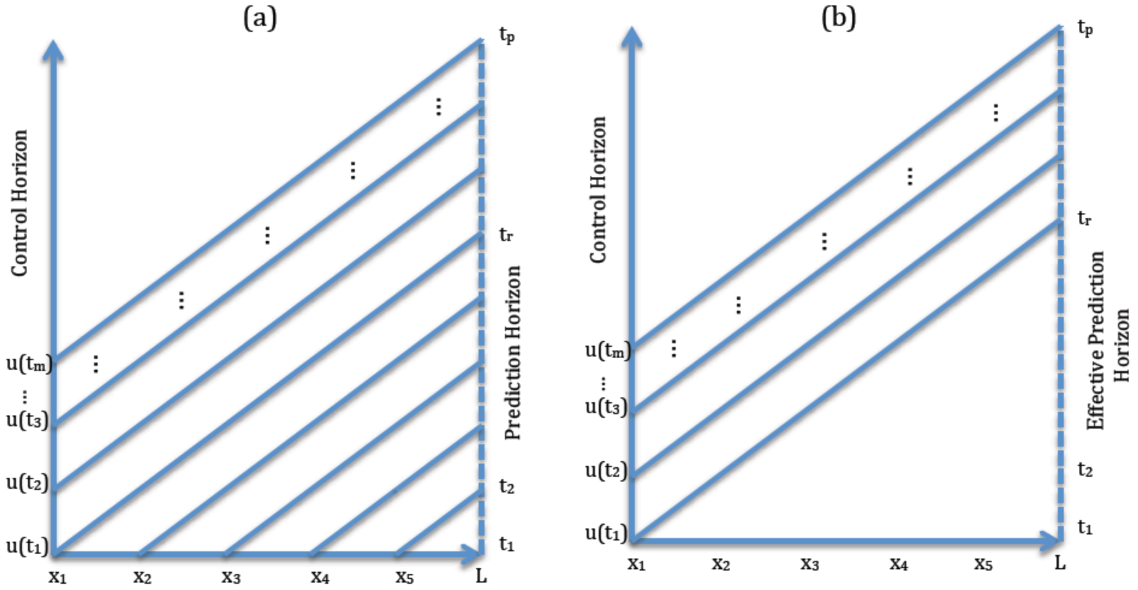

Figure 3.5: Typical characteristic lines for a boundary control problem, (a) total characteristic lines, (b) the effective characteristic lines.

Figure 3.6 is used for the spatially uniform control problem where control actuations are uniformly applied to a tube along its domain. If there are both the spatially uniform and boundary control problems, Figure 3.6 shows the characteristic lines, prediction horizons and control actions with respect to time and length. As can be seen in Figure 3.6, u_1 is the control action that is applied to the boundary of the tube, and u_2 is uniformly applied to the domain of the tube .

3.2.1 Nonlinear Model Predictive Control (NMPC)

NMPC belongs to the class of the optimal controllers using optimization algorithms to find the best control actions for a system. In addition, in large-scale control systems, model-based controllers like MPC are usually preferred to non-model based controllers (e.g. PID controllers) due to the fact that such model-based controllers can efficiently cope with multi-variable nonlinear systems subject to constraints [56–60]. NMPC deploys the original nonlinear model of the process with a set of the intermittently measured process variables in an iterative procedure to solve a nonlinear optimization problem to control the process.

Figure 3.7 depicts the basic idea of MPC. The reference can be assumed to be

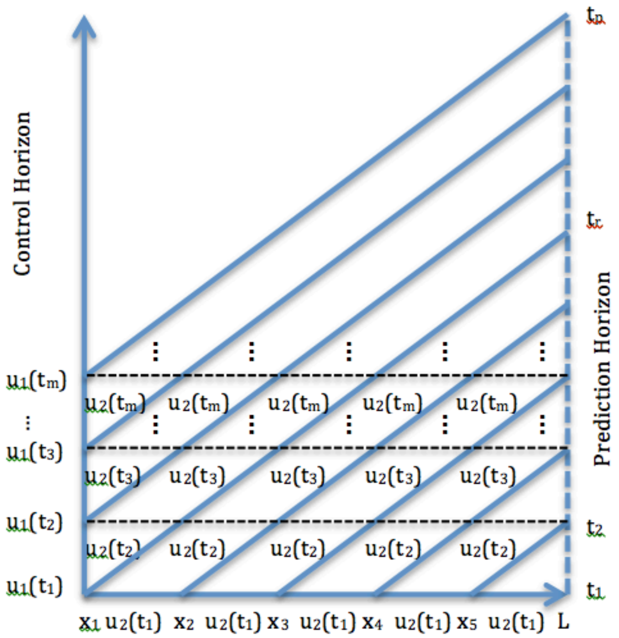

Figure 3.6: Typical characteristic lines for spatially uniform and boundary control problems.

constant, at least within a certain horizon. Starting from the current values of the states of a system and any given control action sequence (u), a prediction trajectory ($\hat{y}$) can be calculated into the future. In the most general format, the objective function in continuous time can be defined as in Equation(3.47). The optimization problem for a standard NMPC is shown in Equations(3.47)-(3.52). [61]

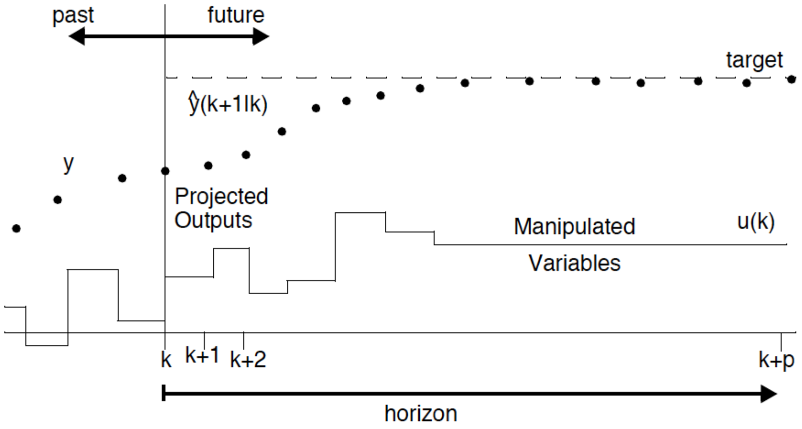

Figure 3.7: Receding horizon concept in MPC

$$\min_{u \in G(w)} \int_{t_k=0}^{t_{k+p}=T} [(\hat{y}(\tau) - r)Q(\hat{y}(\tau) - r) + u(\tau)Ru(\tau)]d\tau \tag{3.47}$$

$$\dot{x}(t) = f(x(t), u(t)) \tag{3.48}$$

$$\hat{y}(t) = h(x(t), u(t)) \tag{3.49}$$

$$u_{min} \leqslant u(t) \leqslant u_{max} \tag{3.50}$$

$$x_{min} \leqslant x(t) \leqslant x_{max} \tag{3.51}$$

$$x(t_k) = \tilde{x}(t_k) \tag{3.52}$$

where: $Q \geqslant 0$ and $R \geqslant 0$ are weighting matrices for states and control actions, respectively; P represents the finite prediction horizon; T stands for the interval of prediction horizon; f denotes the nonlinear model of the process; h represents the nonlinear model of the outputs; r is the target or set-point of the system; u is the control action that belongs to piece-wise constant functions with sampling time w; and x is the predicted trajectory of the state of the system with initial condition $\tilde{x}(t_k)$ that is measured at each sampling time. As mentioned before, the control actions are recalculated at every consecutive time interval. The closed loop stability of the NMPC schemes is eventually based on proper selection of the tuning parameters in the objective function and the prediction and control horizons [60–62]. Furthermore, other factors like the selection of the control horizons are deemed critical in stability of NMPC.

3.2.2 Closed-Loop Stability of CBNMPC

A control law in closed form by using CBMPC cannot be derived for quasilinear PDE systems. Thus, it is not possible to analyze its stability on the basis of the closed-loop transfer functions that can be derived for linear systems. The stability issues are similar to those that exist in the analysis of finite-dimensional NMPC systems. Terminal constraint or terminal cost are usually added to ensure closed-loop stability [63]. In this subsection, the stability of quasilinear systems is investigated when a terminal constraint is added to the objective function. Consider the objective function shown in Equation(3.53) at time instant 'k'. This objective function is equal to the objective function shown in Equation(3.54) that is formed by the summation of subintegrals defined in Equation(3.55). Note that, at each subintegral the value of manipulated variable is constant.

$$I^k = \min_U \int_{t_k=0}^{t_{k+p}=T} (y(x,u) - r)^2 d\tau \tag{3.53}$$

$$I^k = \min_U \sum_{i=1}^{p} I_i^k \tag{3.54}$$

$$I_i^k = \int_{t_{k+i-1}}^{t_{k+i}} (y(\tau, x, u_i) - r)^2 d\tau, \quad i = 1, ..., p \tag{3.55}$$

where: $U = [u_1, ..., u_m = u_{m+1} =, ..., = u_p]$ is the optimal control sequence; x is the state of the system; $y(x,u)$ is the output of the system; r is the set point; and 'm' and 'p' are the control and prediction horizon, respectively. Adding a terminal constraint is one way of ensuring stability for finite-horizon NMPC. A terminal constraint ensures the states or outputs of a system converge to a particular value at the end of the prediction horizon. The following terminal constraints are used to ensure the stability of the CBNMPC:

$$I_p^k \leq min(I_1^k, ..., I_{p-1}^k) \tag{3.56}$$

$$\hat{I}_{p+1}^k \leq I_p^k \tag{3.57}$$

where $\hat{I}_{p+1}^k$ is obtained for the control sequence of $U = [u_1, ..., u_m = u_{m+1} =, ..., = u_{p+1}]$ that was calculated at the time instant 'k'.

Theorem 1 *A CBNMPC that satisfies Equation(3.53) subject to Equations(3.56)-(3.57) is stabilizing if the quasilinear PDE system is controllable at* $y = r$.

Proof. Suppose the optimal control sequence at time instant 'k' is $U = [u_1, ..., u_m = u_{m+1} =, ..., = u_p]$. The control sequence $U = [u_2, ..., u_m = u_{m+1} =, ..., = u_{p+1}]$ is applied to the system at time instant '$k+1'$ without calculating a new optimal control sequence at time instant '$k+1'$. According to Equations(3.56)-(3.57), $\hat{I}_{p+1}^k$ will be smaller than or equal to I_p^k. $\hat{I}^{k+1}$ can be calculated from the following equations:

$$\hat{I}^{k+1} = \sum_{i=2}^{p} I_i^k + \hat{I}_{p+1}^k \tag{3.58}$$

$$= I^k + \hat{I}_{p+1}^k - I_1^k \tag{3.59}$$

and

$$\hat{I}^{k+1} - I^k = \hat{I}_{p+1}^k - I_1^k \tag{3.60}$$

According to Equations(3.56)-(3.57), $\hat{I}_{p+1}^k \leq I_1^k$. As a result, $\hat{I}^{k+1} \leq I^k$, and if the new optimal control sequence at time instant '$k+1'$ is calculated, I^{k+1} will be smaller than or equal to I^k.

If I^k converges to a steady-state positive value, then $I^k = I^{k+1} =, ... = I^{k,ss}$ and $I_i^k \neq 0$. Therefore, the output converges to a steady-state value that is not equal to 'r' under the optimal control sequence U^s. There exists a control sequence U^r that drives the output to the set point at the steady state, and $I^k = I^{k+1} =, ... = I^{k,r}$ because the process is controllable at $y = r$. Therefore, $I^{k,r} < I^{k,ss}$, which contradicts the fact that U^s is the optimal control action. Then, the following inequalities hold:

$$I^{k+1} < I^k \quad if \quad y \neq r \tag{3.61}$$

$$I^{k+1} = I^k \quad if \quad y = r \tag{3.62}$$

Thus, I^k is a non-increasing positive function and the output converges to the set point, so I^k is a Lyapunov function. This proves that the developed CBNMPC is stabilizing. Note that, the operating conditions must not change during simulation. ■

The design of CBNMPC for quasilinear PDE systems does not guarantee stability without limiting constraints. Furthermore, the limiting constraints defined in Equations(3.56)-(3.57) might affect the performance and computational efficiency of CBMPC. Also, the accuracy of the optimization algorithm can affect the stability of CBNMPC. The optimization algorithms are important because for nonconvex problems, the algorithm may get caught in local optima, so it may violate the constraints;

as a result, the stability of closed-lop controller is affected. This issue can be critical when a system exhibits the open-loop unstable behavior for a range of operating conditions.

3.2.3 Case Study

The catalytic packed-bed reactor used as the case study for the open-loop control technique is also considered as the case study for this section.

The solution of the eigenvalue problem of the operator '$\Re'$ defined in Equation(3.63) is similar to that of Equation(2.34) with '$L = 1'$. Equations(3.23) and (3.26) are transformed into a set of ODEs using the numerical technique developed in this work. The new set of equations used for the simulation and control are shown in Equations(3.64)-(3.69).

$$
\begin{aligned}
&\Re\phi = \frac{\partial^2 \phi}{\partial z^2} \\
&D(\Re) = \left\{ \phi \in L^2([0,1];R), \quad z = 0, \frac{\partial \phi}{\partial z} = 0, \quad z = 1, \frac{\partial \phi}{\partial z} = 0 \right\}
\end{aligned}
\tag{3.63}
$$

$$
\frac{dT_n^g(t)}{dt} = \frac{1}{\epsilon}(h^g(\bar{T}_n^c - T_n^g) - h_u^g(T_n^g - u)), \quad n = 1, ..., N \tag{3.64}
$$

$$
\begin{aligned}
\frac{dA_m(t)}{dt} &= \lambda_m A_m + B \int_0^1 [e^{\frac{\gamma T^c}{1+T^c}}]\phi_m dz - A_m(h^c + h_u^c) \\
&+ \int_0^1 [h^c \tilde{T^g} + h_u^c u]\phi_m dz, \quad m = 0, .., M
\end{aligned}
\tag{3.65}
$$

$$
\tilde{T^g}(z,t) = T_n^g(t), \quad at \quad z = \tilde{z}_n + ut, \quad n = 1, ..., N, \quad \tilde{T^g}(0,t) = 0 \tag{3.66}
$$

$$
\lambda_0 = 0, \quad \lambda_m = -(m\pi)^2, \quad \phi_0 = 1, \quad \phi_m(z) = \sqrt{2}\cos(m\pi z) \tag{3.67}
$$

$$
T^c(z,t) = \sum_{m=0}^{M} A_m(t)\phi_m(z) \tag{3.68}
$$

$$
\bar{T}_n^c(t) = \sum_{m=0}^{M} A_m(t)\phi_m(\tilde{z}_n + ut), \quad n = 1, ..., N \tag{3.69}
$$

where: λ is the eigenvalue; ϕ is the eigenfunction and A_m is the amplitude of mode 'm'; $\tilde{T^g}$ is a function of gas temperature along the reactor; $\tilde{z}$ is the spatial point; N is the number of spatial points or characteristic lines; and M is the number of eigenmodes. The control objective is to force the catalyst temperature along the reactor to a predefined set point in order to increase the the production rate. The control problem is defined in Equations(3.70)-(3.72). Note that, this is a spatially uniform control problem. Equations(3.64)-(3.69) are used for the simulation with 5 modes and 20 spatial points. Note that, increasing the numbers of modes and spatial points do not change the simulation results significantly.

The control actions are calculated by solving the optimization defined in Equations(3.64)-(3.69). This optimization problem is solved by the function $\backslash fmincon'$ of **MATLAB**. The function $\backslash ode15s'$ of **MATLAB** is used to solve Equations(3.64)-(3.69)

$$\min_{u(t)} I = \int_0^{0.04} \int_0^1 [(T^c - r)'Q(T^c - r) + uRu] dtdz \tag{3.70}$$

$$subject\, to:$$

$$Eqs.\,(3.64) - (3.69) \tag{3.71}$$

$$0 \leq u(t) \leq 0.068 \tag{3.72}$$

where: r is the set point; and the values of Q and R are 1 and 0.001, respectively. Furthermore, one mode and 10 spatial points were chosen to design CBNMPC. Given these numbers of modes and spatial points, good control performance was achieved. In addition, the computation time needed for the calculation of the control actions was reduced. The sampling time was selected to be half of the residence time (0.005) because the dimensionless time constant of system is about 0.1 and the sampling time was selected to be one-twentieth of the time constant of the catalytic packed-bed reactor. The prediction horizon is 6 and the control horizon is 3. The integral terms in Equation(3.65) are calculated by the trapezoidal rule. The results are shown in Figures 3.8-3.9.

As can be seen in Figure 3.9, CBNMPC perfectly forced the catalyst temperature to its set points. The predefined set points for this section are similar to the case study of open-loop technique. The value of the objective function defined in Equation(3.46) is 0.5702, which shows DT obtained slightly better control performance in comparison with the performance obtained by CBNMPC, as should be expected.

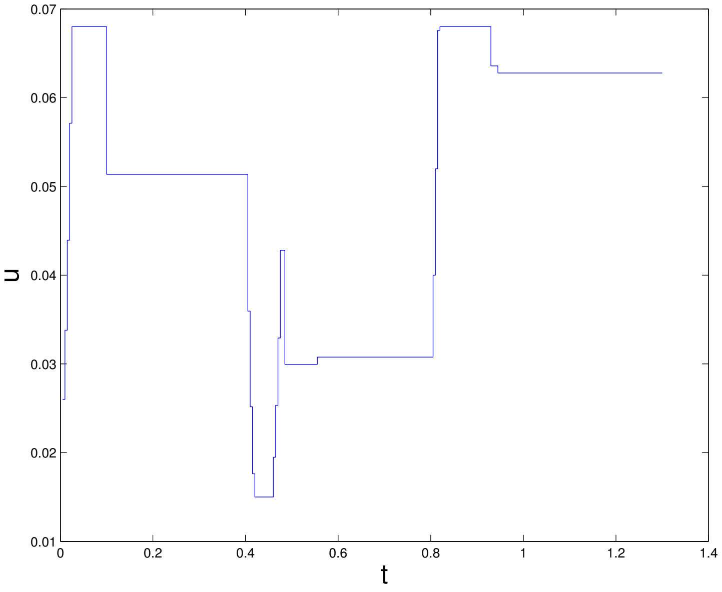

Figure 3.8: Dimensionless control action of catalytic packed-bed reactor with closed-loop control technique.

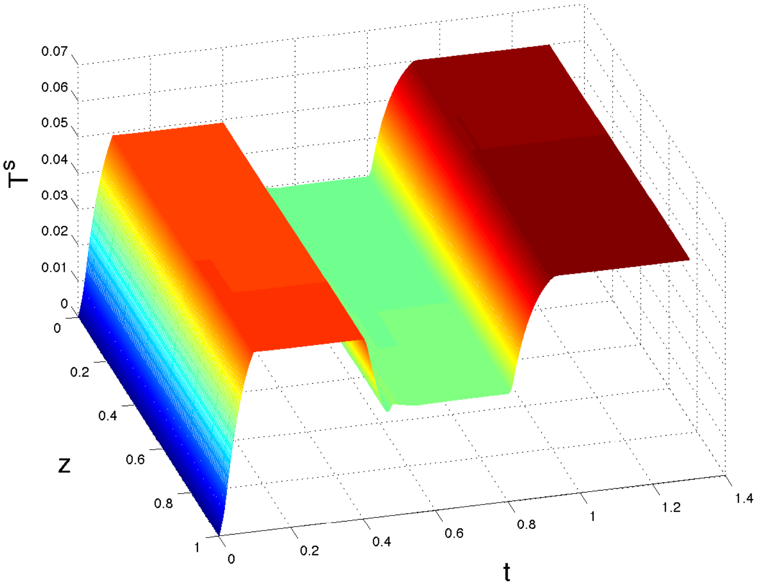

Figure 3.9: Dimensionless catalyst temperature of catalytic packed-bed reactor with closed-loop control technique.

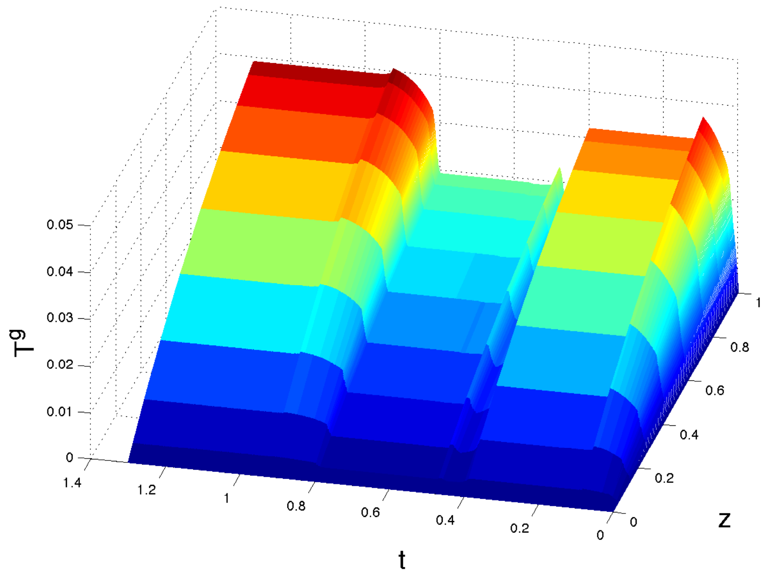

Figure 3.10: Dimensionless gas temperature of catalytic packed-bed reactor with closed-loop control technique.

3.3 Case Study: SCR

The SCR control problem is a boundary control problem. The manipulated variable is initial condition of the concentration of NH_3 (i.e. The NH_3 concentration entering the SCR) in Equation(2.45) that is equal to the boundary condition of Equation(2.8) for NH_3 at each sampling time.

Before implementing the proposed control technique, the controllability of the system must be verified. Note that, CBNMPC requires full state feedback, so an observer is needed to implement this control technique. As a result, the observability of the system must be checked to show the implementability of CBNMPC for SCR. In this work, it is supposed that we posses a perfect model, and we aim at achieving the best control performance for SCR. The space velocity frequently changes in SCR, so we use a variable sampling time in order to overcome this problem. This means that the number of spatial points can be considered constant during simulation. Also, all disturbances are measured.

In this case study, CBNMPC and DT are designed for the SCR problem. A PI controller is also designed for comparison purposes. The PI controller is a single-input single-output controller whose input is the ammonia concentration and output is the NO concentration. Finally, the control performance of all controllers are compared.

A scenario that was defined in Table 2.3, is used to check the capability of CB-NMPC in controlling SCR. There are several scenarios in the literature, but the selected scenario is the hardest one to control. In the predefined scenario, the exhaust aftertreatment system is cold when the diesel engine starts to work. Thus, the functionality of SCR catalyst decreases, so it is hard for a controller to make a compromise between NO$_x$ and ammonia slip reduction. We need an advanced controller to reduce the ammonia slip and NO$_x$ emission perfectly.

3.3.1 Controllability and Observability

According to Theorem 1, the controllability of the SCR is an important condition in the stability of designed CBNMPC. The basic requirement for the controllability of a system including Equations(2.8)-(2.15) is that control actuators must intersect each characteristic line, and the controllability condition must be satisfied along each characteristic line [14]. In order to build the controllability matrix, the existing boundary control problem in the SCR is transformed to a spatially uniform control problem using the following state transformation [45]:

$$\bar{c}^{g}_{NH_3} = c^{g}_{NH_3} - u \tag{3.73}$$

$$\dot{\bar{c}}^{g}_{NH_3} = \dot{c}^{g}_{NH_3} - \dot{u} \tag{3.74}$$

$$\frac{du(t)}{dt} = \bar{u} \tag{3.75}$$

As a result, Equations(2.8) for NH$_3$ and (2.11) are replaced by Equations(3.76) and (3.77). In addition, Equation(3.75) is added to the model. Now,there is a spatially uniform control problem, so a basic requirement for the controllability was satisfied. Since, the control actuator intersects all characteristic lines. Some numerical simulations were performed and the results show that the controllability matrix is full rank during the predefined scenario.

$$
\begin{aligned}
\frac{\partial \bar{c}^{g}_{NH_3}(z,t)}{\partial t} &= -v\frac{\partial \bar{c}^{g}_{NH_3}}{\partial z} + \frac{k_c^{NH_3}a}{\epsilon^g}(c^s_{NH_3} - \bar{c}^{g}_{NH_3} - u) - \bar{u} && (3.76)\\
\frac{dc^{s}_{NH_3}(z,t)}{dt} &= \frac{k_c^{NH_3}a}{1-\epsilon^g}(\bar{c}^{g}_{NH_3} + u - c^s_{NH_3}) - \frac{a}{1-\epsilon^g}(R_1 + R_2 + R_3 + R_4 + R5)\\
&\quad - \frac{a}{1-\epsilon^g}(R_{ad} - R_{des}) && (3.77)
\end{aligned}
$$

The basic requirement for the observability of a system including Equations(2.8)-(2.15) is that measurements must intersect each characteristic line. Then the observability condition can be satisfied along each characteristic line [14]. NO$_x$ and ammonia concentrations, gas temperature, and solid temperature are measured at the inlet and outlet of SCR, so the basic requirement was satisfied, as the sensors placed at the outlet of SCR intersect all characteristic lines. Some numerical simulations were performed and the results show that the observability matrix is full rank during the predefined scenario.

3.3.2 Design of Open-Loop Controller (DT) for SCR

The open-loop control problem is specified so as to achieve the best control performance for the SCR. The algebraic equations obtained from the transformation of Equations(2.8)-(2.15) are shown in Equations(3.78)-(3.97).

$$
\begin{aligned}
&\sum_{j=1}^{M}\bar{c}^{k,g}_{pj}\frac{d\bar{\theta}_{jq}(\hat{t})}{d\hat{t}} = \tau\left(-\frac{v}{L}\sum_{i=1}^{N}\bar{c}^{k,g}_{iq}\frac{d\bar{\varphi}_{ip}(\hat{z})}{d\hat{z}} + \frac{\bar{k}^{k}_{c,pq}a}{\epsilon^g}(\bar{c}^{k,s}_{pq} - \bar{c}^{k,g}_{pq})\right)\\
&\quad k = NO, NO_2, NH_3, O_2, \quad p = 2,..,N, \quad q = 2,...,M && (3.78)\\
&\sum_{j=1}^{M}\bar{c}^{NO,s}_{pj}\frac{d\bar{\theta}_{jq}(\hat{t})}{d\hat{t}} = \tau\left(\frac{\bar{k}^{NO}_{c,pq}a}{1-\epsilon^g}(\bar{c}^{NO,g}_{pq} - \bar{c}^{NO,s}_{pq}) - \frac{a}{1-\epsilon^g}(0.5\bar{R}_{1,pq} + \bar{R}_{2,pq} - \bar{R}_{5,pq})\right)\\
&p = 1,..,N, \quad q = 2,...,M && (3.79)\\
&\sum_{j=1}^{M}\bar{c}^{NO_2,s}_{pj}\frac{d\bar{\theta}_{jq}(\hat{t})}{d\hat{t}} = \tau\left(\frac{\bar{k}^{NO_2}_{c,pq}a}{1-\epsilon^g}(\bar{c}^{NO_2,g}_{pq} - \bar{c}^{NO_2,s}_{pq}) - \frac{a}{1-\epsilon^g}(0.5\bar{R}_{1,pq} + 0.75\bar{R}_{3,pq})\right)\\
&p = 1,..,N, \quad q = 2,...,M && (3.80)
\end{aligned}
$$

$$\sum_{j=1}^{M} \bar{c}_{pj}^{NH_3,s} \frac{d\bar{\theta}_{jq}(\hat{t})}{d\hat{t}} = \tau \Bigg(\frac{\bar{k}_{c,pq}^{NH_3} a}{1-\epsilon^g} (\bar{c}_{pq}^{NH_3,g} - \bar{c}_{pq}^{NH_3,s}) - \frac{a}{1-\epsilon^g} (\bar{R}_{1,pq} + \bar{R}_{2,pq} + \bar{R}_{3,pq} + \bar{R}_{4,pq}$$

$$+ \bar{R}_5) - \frac{a}{1-\epsilon^g} (\bar{R}_{ad,pq} - \bar{R}_{des,pq}) \Bigg), \quad p = 1,..,N, \quad q = 2,...,M \tag{3.81}$$

$$\sum_{j=1}^{M} \bar{c}_{pj}^{O_2,s} \frac{d\bar{\theta}_{jq}(\hat{t})}{d\hat{t}} = \tau \left(\frac{\bar{k}_{c,pq}^{O_2} a}{1-\epsilon^g} (\bar{c}_{pq}^{O_2,g} - \bar{c}_{pq}^{O_2,s}) - \frac{a}{1-\epsilon^g} (\frac{3}{4} \bar{R}_{4,pq} + \frac{5}{4} \bar{R}_{5,pq}) \right)$$

$$p = 1,..,N, \quad q = 2,...,M \tag{3.82}$$

$$\sum_{j=1}^{M} \bar{\psi}_{pj}^{NH_3} \frac{d\bar{\theta}_{jq}(\hat{t})}{d\hat{t}} = \tau \left(\frac{1}{\Psi_{NH_3}^{cap}} (\bar{R}_{ad,pq} - \bar{R}_{des,pq} - a\bar{R}_{4,pq}) \right)$$

$$p = 1,..,N, \quad q = 2,...,M \tag{3.83}$$

$$\sum_{j=1}^{M} \bar{T}_{pj}^{g} \frac{d\bar{\theta}_{jq}(\hat{t})}{d\hat{t}} = \tau \left(-\frac{v}{L} \sum_{i=1}^{N} \bar{T}_{iq}^{g} \frac{d\bar{\varphi}_{ip}(\hat{z})}{d\hat{z}} + \frac{\bar{k}_{h,pq} a}{\rho^g cp^g \epsilon^g} (\bar{T}_{pq}^{s} - \bar{T}_{pq}^{g}) \right)$$

$$p = 2,..,N, \quad q = 2,...,M \tag{3.84}$$

$$\sum_{j=1}^{M} \bar{T}_{pj}^{s} \frac{d\bar{\theta}_{jq}(\hat{t})}{d\hat{t}} = \tau \Bigg(\frac{\lambda^s}{\rho^s cp^s L^2} \sum_{i=1}^{N} \bar{T}_{iq}^{s} \frac{d^2\bar{\varphi}_{ip}(\hat{z})}{d\hat{z}^2} - \frac{\bar{k}_{h,pq} a}{\rho^s cp^s (1-\epsilon^g)} (\bar{T}_{pq}^{s} - \bar{T}_{pq}^{g})$$

$$- \frac{k_{ext} a_{ext}}{\rho^s cp^s (1-\epsilon^g)} (\bar{T}_{pq}^{s} - T^{ext}) - \frac{1}{\rho^s cp^s (1-\epsilon^g)} \sum_{j=1}^{5} \Delta H_j \bar{R}_{j,pq} \Bigg)$$

$$p = 2,..,N-1, \quad q = 2,...,M \tag{3.85}$$

$$c_k^f(\hat{z},\hat{t}) = \sum_{i=1}^{N} \sum_{j=1}^{M} \bar{c}_{ij}^{k,f} \varphi_i(\hat{z}) \theta_j(\hat{t}), \quad k = NO, NO_2, NH_3, O_2, \quad f = g, s \tag{3.86}$$

$$T^k(\hat{z},\hat{t}) = \sum_{i=1}^{N} \sum_{j=1}^{M} \bar{T}_{ij}^{k} \varphi_i(\hat{z}) \theta_j(\hat{t}), \quad f = g, s \tag{3.87}$$

$$\psi_{NH_3}(\hat{z},\hat{t}) = \sum_{i=1}^{N} \sum_{j=1}^{M} \bar{\psi}_{ij}^{NH_3} \varphi_i(\hat{z}) \theta_j(\hat{t}) \tag{3.88}$$

$$u(\hat{t}) = \sum_{j=1}^{M} \bar{u}_j \theta_j(\hat{t}) \tag{3.89}$$

$Boundary\, Conditions:$

$(\hat{z} = 0)$

$$\bar{c}_{1q}^{k,g} = c_k^g(0, t(q)), \quad k = NO, NO_2, O_2, \quad q = 2,...,M \tag{3.90}$$

$$\bar{c}_{1q}^{NH_3,g} = \bar{u}_q, \quad q = 2,...,M \tag{3.91}$$

$$\bar{T}^{g}_{1q} = T^{k}(0, t(q)), \quad q = 2, ..., M \tag{3.92}$$

$$\sum_{i=1}^{N} \bar{T}^{s}_{iq} \frac{d\bar{\varphi}_{i1}(\hat{z})}{d\hat{z}} = 0, \quad q = 2, ..., M \tag{3.93}$$

$$(\hat{z} = 1)$$

$$\sum_{i=1}^{N} \bar{T}^{s}_{iq} \frac{d\bar{\varphi}_{iN}(\hat{z})}{d\hat{z}} = 0, \quad q = 2, ..., M \tag{3.94}$$

$$Initial\,Conditions:$$

$$\bar{c}^{k,f}_{p1} = 0, \quad k = NO, NO_2, NH_3, O_2, \quad f = g, s \quad p = 1, ..., N \tag{3.95}$$

$$\bar{T}^{f}_{p1} = 300, \quad f = g, s \quad p = 1, ..., N \tag{3.96}$$

$$\bar{u}_1 = 0 \tag{3.97}$$

where: $\bar{c}$, $\bar{\psi}$,$\bar{T}$, and $\bar{u}$ are the coefficients of the Lagrange polynomials; N is the number of spatial points; and M is the number of temporal points. The superscripts ‘g' and ‘s'represent gas and solid phases, respectively. The heat and mass transfer coefficients in each spatio-temporal point(i,j) are shown in Table 3.2. In addition, the reaction rates in each spatio-temporal point(i,j) are shown in Equations(3.98)-(3.104)

Table 3.2: Mass and heat transfer coefficients in each spatio-temporal point(i,j) for SCR

Parameter	Equation	Unit
$\bar{k}_{h,ij}$	$= 19 + 0.1748\bar{T}^{g}_{ij} - 18.318 * 10^{-6}(\bar{T}^{g}_{ij})^{2}$	$[Wm^{-2}K^{-1}]$
$\bar{k}^{NO}_{c,ij}$	$= 2.745 * 10^{-6}(\bar{T}^{g}_{ij})^{1.75}$	$[ms^{-1}]$
$\bar{k}^{NO_2}_{c,ij}$	$= 2.212 * 10^{-6}(\bar{T}^{g}_{ij})^{1.75}$	$[ms^{-1}]$
$\bar{k}^{NH_3}_{c,ij}$	$= 2.959 * 10^{-6}(\bar{T}^{g}_{ij})^{1.75}$	$[ms^{-1}]$
$\bar{k}^{O_2}_{c,ij}$	$= 2.399 * 10^{-6}(\bar{T}^{g}_{ij})^{1.75}$	$[ms^{-1}]$

$$\bar{R}_{1,ij} = 2.53 * 10^6 e^{\frac{-3007}{\bar{T}^s_{i,j}}} \frac{\bar{c}_{ij}^{NO,s}\bar{c}_{ij}^{NO_2,s}\bar{c}_{ij}^{NH_3,s}}{1 + 1.2042 * 10^{-3}\bar{c}_{ij}^{NH_3,s}} \tag{3.98}$$

$$\bar{R}_{2,ij} = 2.36 * 10^8 e^{\frac{-7151}{\bar{T}^s_{i,j}}} \frac{\bar{c}_{ij}^{NO,s}\bar{c}_{ij}^{NH_3,s}}{1 + 1.2042 * 10^{-3}\bar{c}_{ij}^{NH_3,s}} \tag{3.99}$$

$$\bar{R}_{3,ij} = 7.56 * 10^8 e^{\frac{-8507}{\bar{T}^s_{i,j}}} \frac{\bar{c}_{ij}^{NO_2,s}\bar{c}_{ij}^{NH_3,s}}{1 + 1.2042 * 10^{-3}\bar{c}_{ij}^{NH_3,s}} \tag{3.100}$$

$$\bar{R}_{4,ij} = 1.32 * 10^7 e^{\frac{-15034}{\bar{T}^s_{i,j}}} \bar{\psi}_{ij}^{NH_3} \tag{3.101}$$

$$\bar{R}_{5,ij} = 9.11 * 10^{10} e^{\frac{-14503}{\bar{T}^s_{i,j}}} \frac{\bar{c}_{ij}^{O_2,s}\bar{c}_{ij}^{NH_3,s}}{(1 + 1.2042 * 10^{-3}\bar{c}_{ij}^{NH_3,s})(1 + 1.5053 * 10^{-3}\bar{c}_{ij}^{O_2,s})} \tag{3.102}$$

$$\bar{R}_{ad,ij} = 0.82 c^s_{NH_3,n}(1 - \bar{\psi}_{ij}^{NH_3}) \tag{3.103}$$

$$\bar{R}_{des,ij} = 3.67 * 10^6 e^{\frac{-12992(1 - 0.310\bar{\psi}_{ij}^{NH_3})}{\bar{T}^s_{i,j}}} \bar{\psi}_{ij}^{NH_3} \tag{3.104}$$

M and N were selected to be 120 and 40, respectively. The spatial and temporal points are roots of the Chebyshev polynomial. The values τ and L are 13.84 seconds and 12 centimeters, respectively. The control actions are calculated by solving the optimization problem shown in Equations(3.105)-(3.108). This optimization problem is solved by the function \`$fmincon'$ of **MATLAB**, and the Newton-Raphson method is used to solve Equations(3.78)-(3.97).

$$\min_{\bar{u}_2,\ldots,\bar{u}_M} I = \int_0^1 [yQ\acute{y} + uR\acute{u}]d\hat{t}$$

$$y = [\tilde{c}^g_{NO}, \tilde{c}^g_{NO_2}, \tilde{c}^g_{NH_3}] \tag{3.105}$$

$$\tilde{c}^g_k(q) = \bar{c}^{k,g}_{N,q}, \quad k = NO, NO_2, NH_3, \quad q = 1, ..., M \tag{3.106}$$

$$Subject\,to:$$

$$Eqs.(3.78) - (3.97) \tag{3.107}$$

$$0 \leq \bar{u}_q \leq 700, \quad q = 2, ..., M \tag{3.108}$$

where: $\tilde{c}^g$ is a function of the temporal points for the the concentration of gas components; and the values of Q and R are 1 and 0.001, respectively.

3.3.3 Design of Closed-Loop Controller (CBNMPC) for SCR

In this section, a CBNMPC is designed for SCR. The optimization problem defined in Equations(3.109)-(3.111) is solved to obtain the control actions. The optimization problem is solved by using **MATLAB**'s $\backslash fmincon'$ function. The function $\backslash ode15s'$ of **MATLAB** is used to solve the all ODEs. The performance index and equations used to calculate control actions are shown in

$$\begin{aligned}
&\min_{u(t)=c^g_{NH_3}(z=0,t)} I = \int_0^T [yQ\acute{y} + uR\acute{u}]dt \\
&y = [c^g_{NO}(z=L,t), c^g_{NO_2}(z=L,t), c^g_{NH_3}(z=L,t)] && (3.109)\\
&Subject\,to: \\
&Eqs.(2.45)-(2.56)\,and\,Eqs.(2.64)-(2.70) && (3.110)\\
&0 \le u(t) \le 700 && (3.111)
\end{aligned}$$

where: T is the prediction horizon; and the values of Q and R are 1 and 0.001, respectively. The sampling time is one-fifth of the residence time. The prediction and control horizons were chosen as 10 and 3, respectively. Equations(2.45)-(2.56) and Equations(2.64)-(2.70) with 60 modes and 90 spatial points were used to design CBNMPC. These values were selected based on numerical simulations. The integral terms in Equation(2.52) are calculated by the trapezoidal rule.

3.3.4 Design of PI controller

In this section, a PI controller is designed for SCR. The control action u is calculated by Equation(3.112).

$$u(t) = K_c e(t) + K_I \int_0^t e(t)dt, \quad 0 \le u(t) \le 700 \tag{3.112}$$

where e is the outlet concentration of NO, and K_c and K_I are proportional and integral gains of the controller, respectively. The proportional and integral gains of the controller were selected 4.5 and 3.5, respectively. These values are obtained by trial and error simulations. The PI controller uses the measurement of the outlet concentration of NO.

3.3.5 Result and Discussion

The three-dimensional profiles of gas and solid temperatures obtained by the controllers are shown in Figures 3.11 and 3.12. As can be seen, the inlet gas temperature changes with time due to the changes in the operating mode of the diesel engine in the drive cycle defined in Table 2.3. The inlet gas temperature decreases rapidly because the initial solid temperature is low. Note that, the cold solid consumes the most of the gas energy in the first quarter of the length of SCR. Then, the temperatures of the both gas and solid become similar. The solid temperature at the entrance of SCR is high, and the solid temperature decreases toward the exit of the SCR. This stems from the fact that heat conductivity of the monolith reactor is low, so a small part of the heat absorbed from the gas phase at the entrance of SCR, is conducted down the length of SCR; Thus, there is a big difference in the solid temperature between the inlet and the outlet of SCR. Note that, the solid temperature gradually increases during operation.

The profiles of manipulated variable (i.e., the inlet concentration of ammonia), for each controller are shown in Figure 3.13. As can be seen, The control action obtained by the PI controller remains at the upper bound for most of the simulated operation. The profiles of the outlet concentration of NO obtained by CBNMPC, DT and PI controllers are shown in Figure 3.14. As can be seen, when the solid temperature is low, the concentration of NO increases. After 6 seconds: the solid temperature rises; the conversion of NO increases; and the controllers can effectively minimize the outlet concentration of NO. The solid temperature has a significant influence on the performance of SCR, and, it consequently affects the performances of the controllers. CBNMPC and DT show the better performance compared to the performance achieved by the PI controller when solid is cold. Figure 3.15 shows the profiles of the outlet concentration of NO_2. Like the outlet concentration of NO, CBNMPC and DT achieve the better control performances compared to the performance obtained by the PI controller when the solid phase is cold. When the temperature

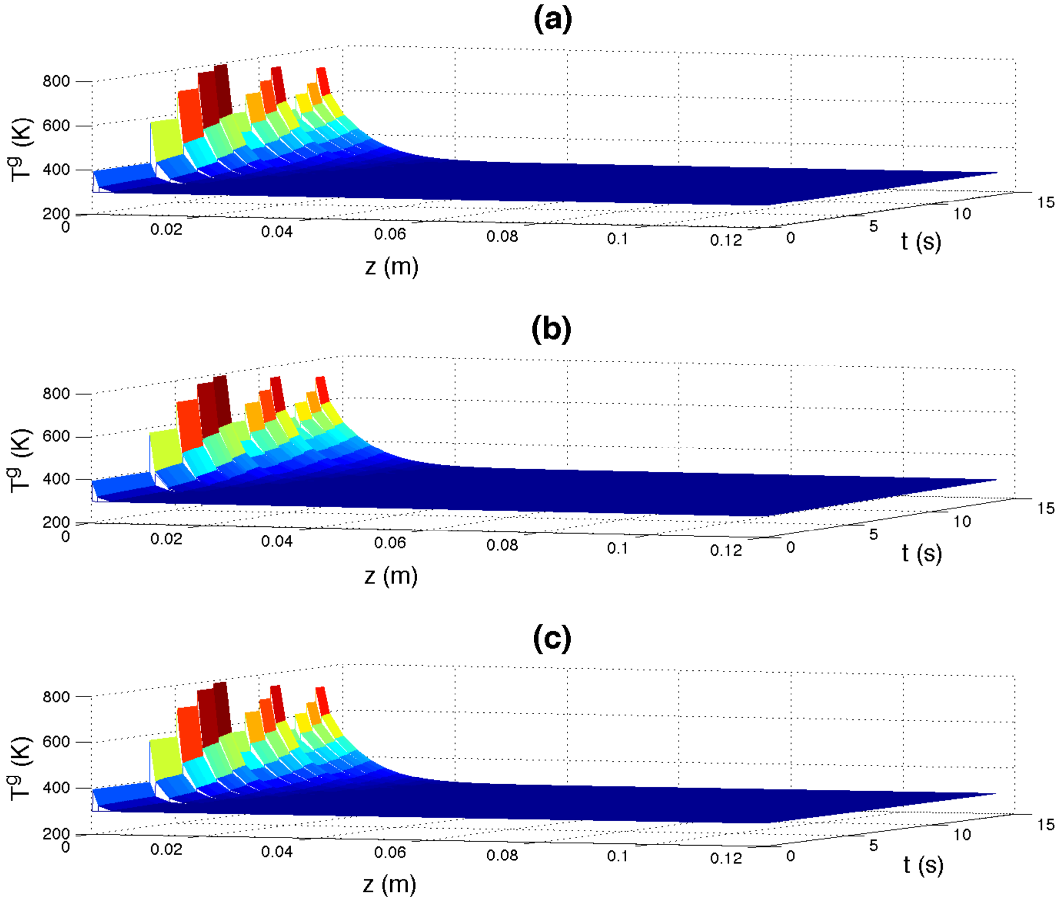

Figure 3.11: Three-dimensional profiles of gas temperature: (a) profile obtained by CBNMPC; (b) profile obtained by DT; (c) profile obtained by PI.

of the solid increases, all controllers can minimize the outlet concentration of NO_2. Figure 3.16 shows the profiles of the outlet concentration of NH_3. It is noteworthy that NH_3 is more harmful than NO_x to the human health, so it is vital to keep the outlet concentration of NH_3 as low as possible. Contrary to CBNMPC and DT, the PI controller is not able to minimize the outlet concentration of NH_3 for most of the simulation. In industry, an additional exhaust aftertreatment component is required to reduce ammonia slip. As expected, DT obtained the best control performance. CBNMPC achieved a satisfactory performance, keeping the outlet concentration of NH_3 lower than 20 ppm.

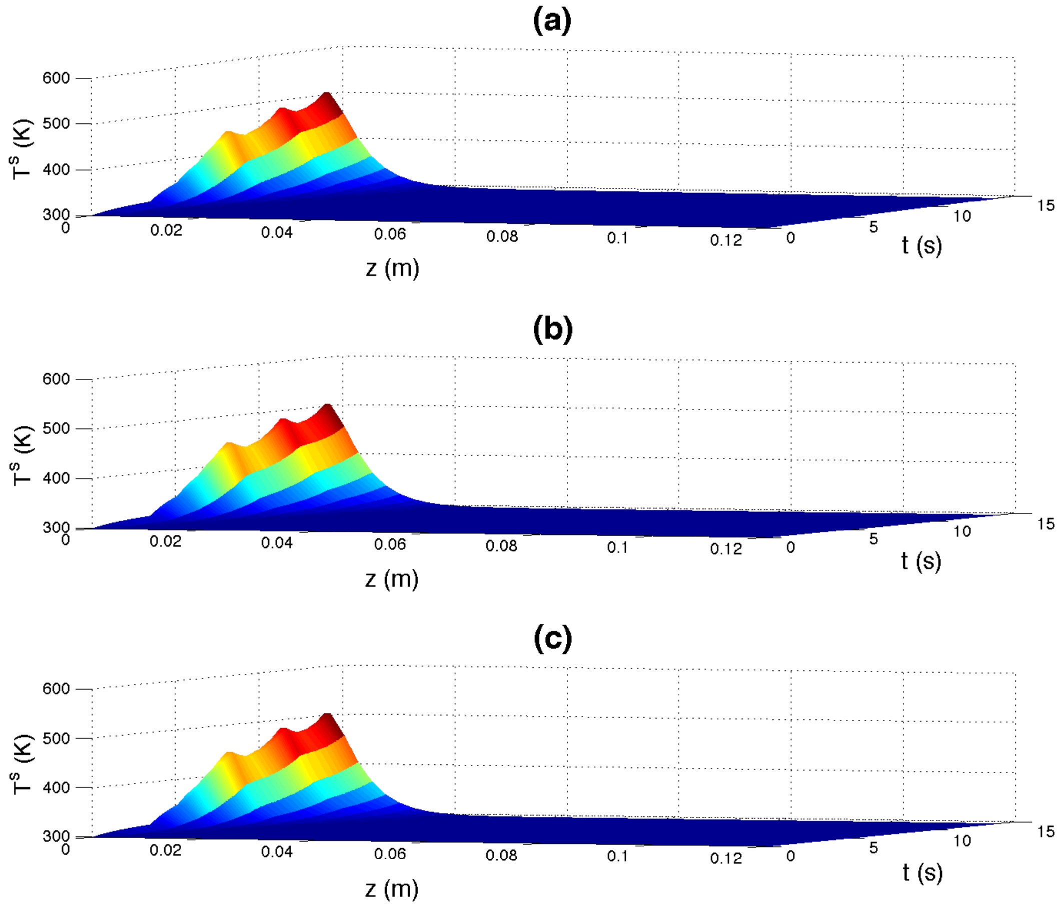

Figure 3.12: Three-dimensional profiles of solid temperature: (a) profile obtained by CBNMPC; (b) profile obtained by DT; (c) profile obtained by PI.

The value of the objective function defined in Equation(3.113), is used to compare the control performance of all controllers. The values of the performance index defined in Equation(3.113), which were obtained by DT, CBNMPC and PI controllers are 8.7638×10^3, 2.0421×10^4, and 8.9176×10^4, respectively. As expected, DT has the best control performance and the PI controller has the worst control performance. These values shows that the distributed parameter controller proposed in this work (CBNMPC) can achieve a reliable and satisfactory control performance that reduces the outlet concentrations of NH_3 and NO_x lower than 20 and 50 ppm, respectively.

$$
\begin{aligned}
&I = \int_0^{13.84} yQ\acute{y}dt \\
&y = [c^g_{NO}(z=L,t), c^g_{NO_2}(z=L,t), c^g_{NH_3}(z=L,t)] \qquad (3.113)
\end{aligned}
$$

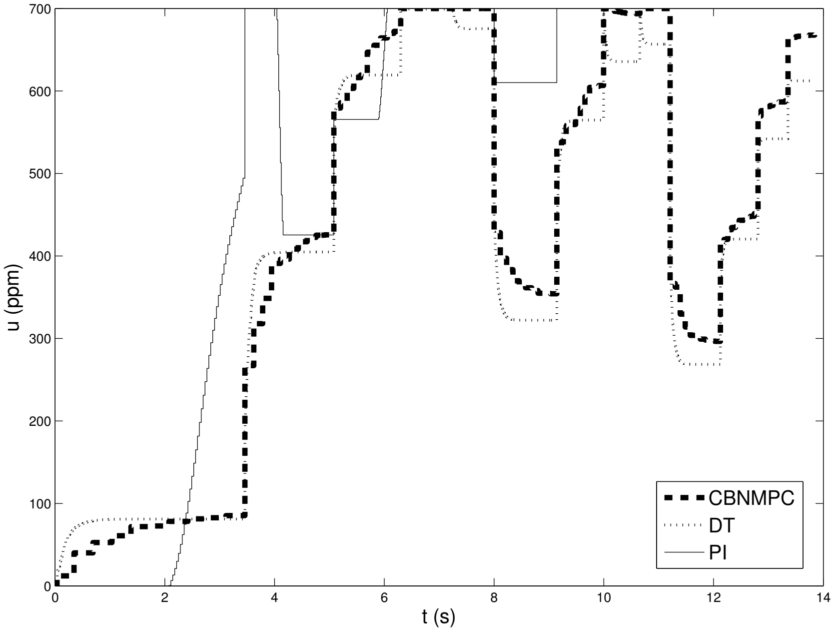

Figure 3.13: Profiles of manipulated variable.

Figures (3.17)-(3.19) show the three-dimensional profiles of outlet concentrations of NO, NO_2 and NH_3 obtained by the controllers, respectively. As can be seen, the most of the reactions occur in the first quarter of the length of SCR where the temperature of solid is high. Thus, the conversion is high and the inlet concentrations of components decrease sharply at the first quarter of the length of SCR (from the inlet to a point 3 centimeters from the entrance of the SCR). The profiles of concentrations does not change noticeably from the inlet to a point 3 centimeters from the entrance of the SCR.

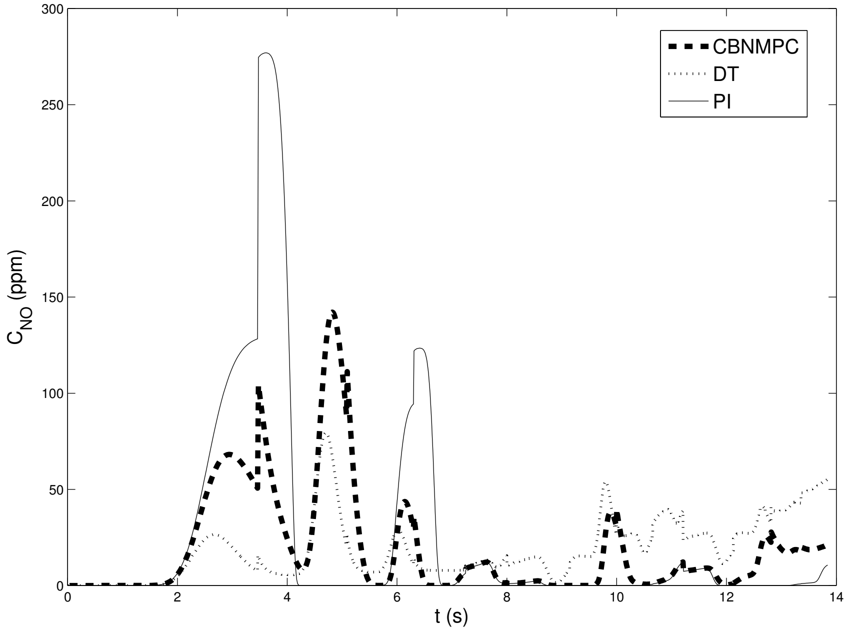

Figure 3.14: Profiles of outlet concentration of NO.

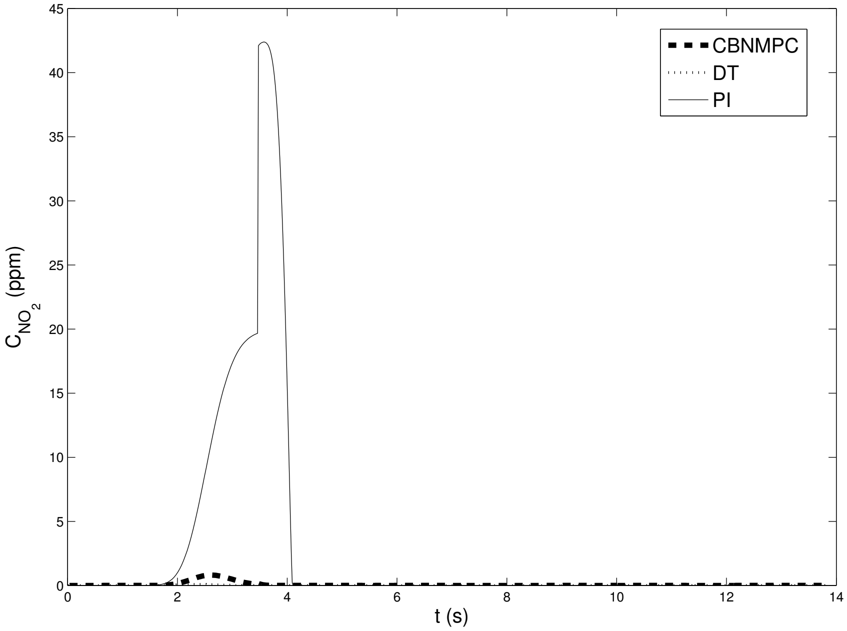

Figure 3.15: Profiles of outlet concentration of NO_2.

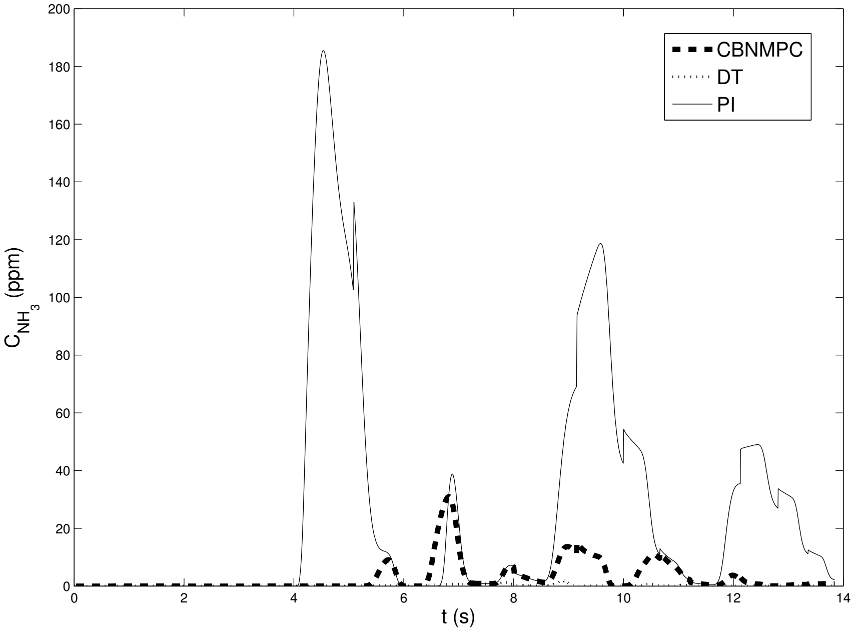

Figure 3.16: Profiles of outlet concentration of NH_3.

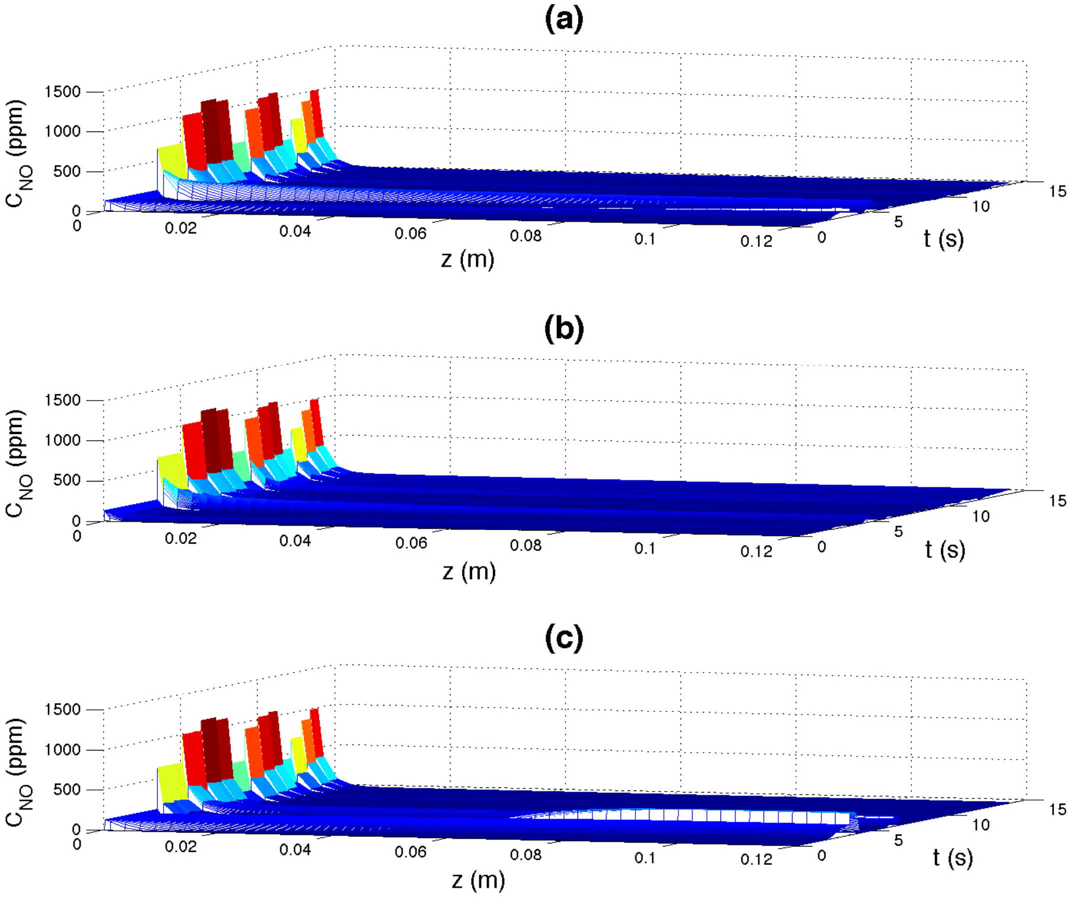

Figure 3.17: Three-dimensional profiles of concentration of NO: (a) profile obtained by CBNMPC; (b) profile obtained by DT; (c) profile obtained by PI.

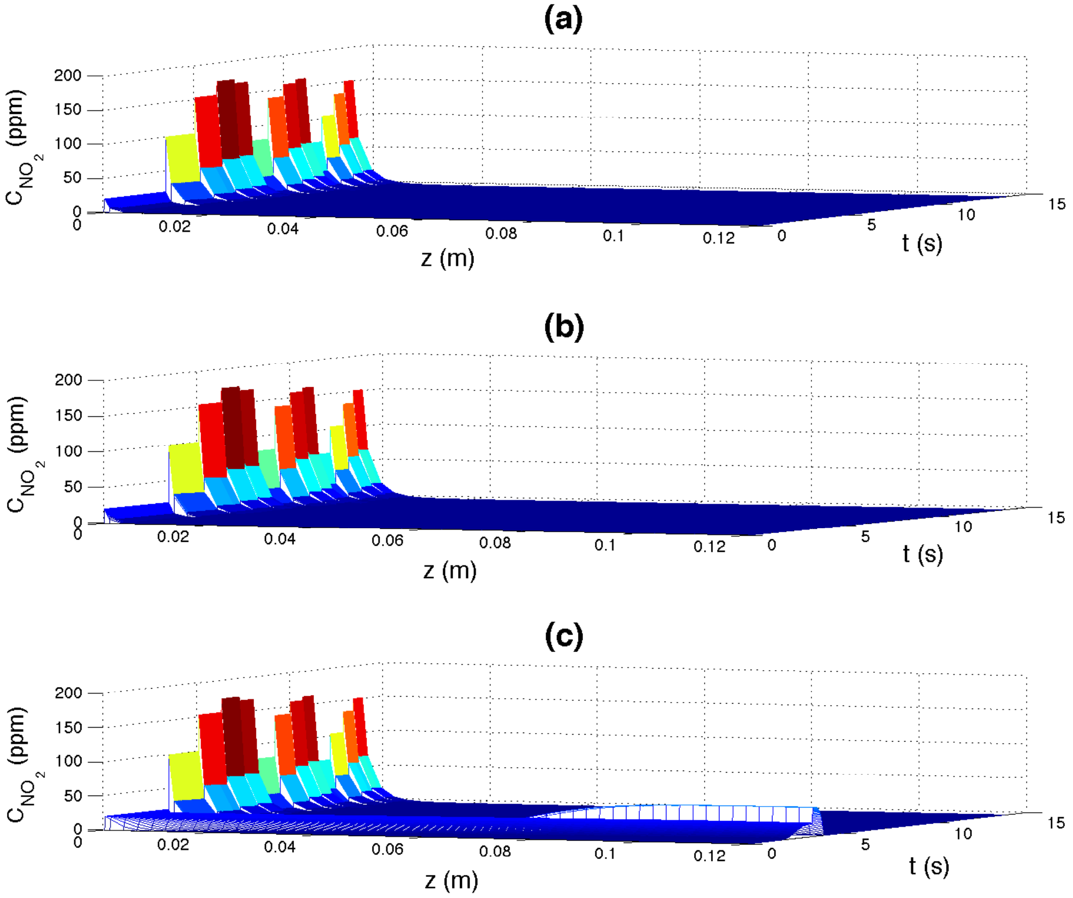

Figure 3.18: Three-dimensional profiles of concentration of NO_2: (a) profile obtained by CBNMPC; (b) profile obtained by DT; (c) profile obtained by PI.

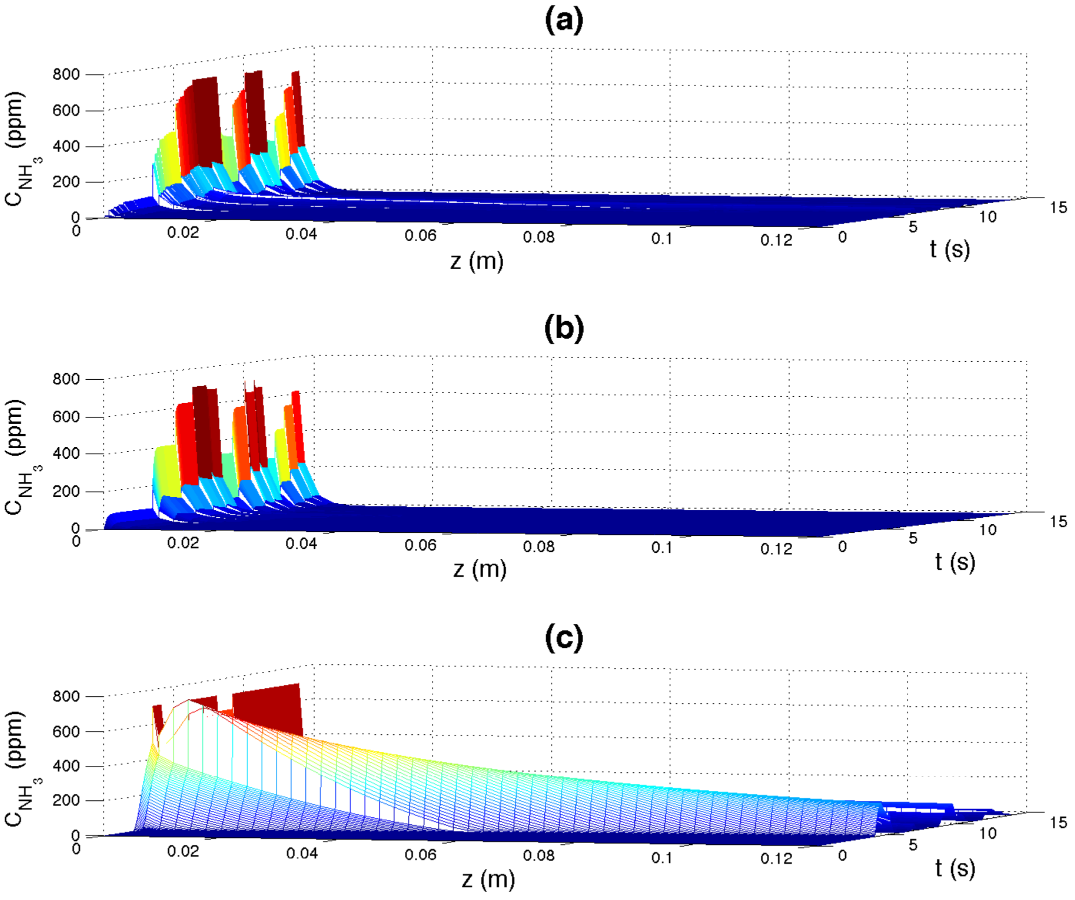

Figure 3.19: Three-dimensional profiles of concentration of NH_3: (a) profile obtained by CBNMPC; (b) profile obtained by DT; (c) profile obtained by PI.

Chapter 4

Summary and Conclusions

The main focus of this work is to design a distributed parameter controller for a SCR. Models for a SCR consist of coupled hyperbolic and parabolic PDEs, and some ODEs. The hyperbolic PDEs represent the concentrations of the gas phase components and the gas phase temperature. The parabolic PDE represents the solid temperature. A set of ODEs represent the concentrations of components that exist in the solid phase. Since, this is a complex system with the nonlinear ODEs and the quasilinear PDEs, a reliable numerical method is needed to design a model-based controller. During first stage of work, a numerical method is proposed that combines the method of characteristics, which is used for solving hyperbolic PDEs, and spectral decomposition, which is used to order reduction of parabolic PDEs, was developed. These methods are used to exactly transform PDEs to a finite set of ODEs. The resulting set of ODEs are solved along characteristic lines defined by the hyperbolic PDEs. The transformed model equations are highly nonlinear and include some nonconvex terms. Since, the operating conditions change during the drive cycle defined in this work, there is no steady state condition during simulation. As a result, it is required a powerful control technique that is able to deal with such a complex system. CBNMPC is a closed-loop control approach that can be practically applied to various systems. This control technique contains nonconvex optimization problem, which requires powerful solution algorithms, such as, the function '*fmincon*' of **MATLAB**. CBNMPC was designed for SCR the boundary control problem in the SCR. Ammonia flow to the SCR inlet is considered as the manipulated variable. The control objective is to minimize the outlet concentration of the NO_x emission and the ammonia slip. Furthermore, an open-loop dynamic optimization problem was formulated to determine the best control performance that can be achieved in the SCR. The open-loop control technique was developed assuming perfect information of the drive cycle defined in this work. The orthogonal collocation technique was used to discretize the SCR model. Lagrange polynomials was used as the orthogonal polynomial. In addition, the temporal and spatial points were selected roots of the Chebyshev polynomials. Also, a PI controller was designed. The designed PI controller uses the measurement of the outlet concentrations of NO. Finally, the performance of each control approach was determined via simulation and compared using the obtained performance indices. The performance index shows that CBNMPC is significantly better than performance of the PI controller. According to the defined performance index, the control performances of DT, CBNMPC and PI controllers are 8.7638×10^3, 2.0421×10^4, and 8.9176×10^4, respectively. The simulation study shows that CBNMPC is a viable candidate for substantially improving SCR control performance. Furthermore, distributed parameter controllers like CBNMPC can obviate the need for installing AOC in the exhaust aftertreatment systems, which will reduce costs of exhaust aftertreatment systems.

Based on performing several numerical simulations, 100 modes and 180 characteristic lines could capture the main dynamics of SCR, and increasing these values did not have any significant effect on the results obtained by simulation. The number of modes was selected as 60, and the number of the characteristic lines was chosen to be 100 for the design of CBNMPC. Also, the number of temporal and spatial points for the design of DT were selected to be 120 and 40, respectively.

In the development of the proposed CBNMPC, we require that the concentrations and temperatures are known along the reactor. This requires an observer to estimate the values of the concentrations and temperatures along SCR. Note that, the heat conduction coefficient and heat capacity of monolith reactor were selected constant. In reality, these parameters are a function of temperature, and they change during the simulation. As a result, the eigenvalues and eigenfunctions obtained by using the spectral decomposition change during simulation.

4.1 Directions for Future Work

There are several options for the future work that some conspicuous ones are mentioned as follows:

- The exhaust aftertreatment systems in diesel-powered vehicles includes several components, such as, DOC and DPF, so one option for future work is to design a network of controllers like coordinated distributed NMPC for SCR.
- The current design does not consider plant-model mismatch. Another option for future work is considering some uncertainties in the modelling of SCR (e.g., uncertainties in the reaction rates and heat and mass transfer coefficients). A robust control techinque can be used or developed for SCR.
- The observer design for the SCR would be valuable because we need an observer to estimate the concentrations and temperatures along SCR.
- The design of CBNMPC with temperature-dependent heat conduction coefficient and heat capacity for the monolith reactor to investigate the effects of this property on the SCR control performance.
- SCR control performance can be improved by heating SCR up to an optimal temperature. This requires a compromise between the cost of energy needed for heating and the reduction of the NO_x emissions and ammonia slip. Also, modelling of a heat exchanger reactor for a SCR and the control of it would be challenging.
- The utilization of the proper orthogonal decomposition (POD) or the Karhunen-Loeve (K-L) decomposition for obtaining a low-dimensional dynamic model of SCR instead of using the method of characteristics and spectral decomposition. We can develop an off-line model for SCR in order to reduce the computation time needed to calculate control actions for such a fast system.

Bibliography

[1] US Department of Energy, "Diesel Power : Clean Vehicles for Tomorrow," 2010. [Online]. Available: http://www.eere.energy.gov

[2] Manufacturers of Emission Controls Association, "Emission Control Technologies for Diesel-Powered Vehicles," Tech. Rep. December, 2007.

[3] D. Chatterjee, M. Weibel, B. Krutzsch, P. Koc, I. Nova, and E. Tronconi, "Current Status of Modeling Lean Exaust Gas Aftertreatment Catalysts," *Advances in Chemical Engineering*, vol. 33, no. 07, pp. 103–211, 2008.

[4] E. Alfieri, "Emissions-Controlled Diesel Engine," PhD, Swiss Federal Institute of Technology Zurich, 2009.

[5] T. Akiyoshi, H. Torisaka, H. Yokota, T. Shimizu, H. Ninomiya, and H. Narita, "Development of Efficient Urea-SCR Systems for EPA 2010-Compliant Medium Duty Diesel Vehicles," *SAE International*, 2011.

[6] K. Hirata, N. Masaki, H. Ueno, and H. Akagawa, "Development of Urea-SCR System for Heavy-Duty Commercial Vehicles," vol. 2005, no. 724. Detroit, Michigan: SAE World Congress, 2005.

[7] C. Lambert, G. Cavataio, Y. Cheng, D. Dobson, J. Girard, P. Laing, J. Patterson, and S. Williams, "Urea SCR and DPF System for Tier 2 Diesel Light-Duty Trucks," Tech. Rep., 2006.

[8] M. C. J. Gieshoff, M. Pfeifer, A. Schäfer-Sindlinger and P. C. Spurk,G. Garr and T. Leprince, "Advanced Urea SCR Catalysts for Automotive Applications." Detroit, Michigan: SAE World Congress, 2001.

[9] J. N. Chi and H. F. M. Dacosta, "Modeling and Control of a Urea-SCR Aftertreatment System Reprinted From : Diesel Exhaust Emission Control Modeling," no. 724. Detroit, Michigan: SAE World Congress, 2005.

[10] D. Kryl and P. Koc, "Catalytic Converters for Automobile Diesel Engines with Adsorption of Hydrocarbons on Zeolites," *Industrial and Engineering Chemistry Research*, pp. 9524–9534, 2005.

[11] M. Schejbal, J. Štěpánek, M. Marek, P. Kočí, and M. Kubíček, "Modelling of Soot Oxidation by NO2 in Various Types of Diesel Particulate Filters," *Fuel*, vol. 89, no. 9, pp. 2365–2375, Sep. 2010.

[12] L. Mukadi and R. Hayes, "Modelling the Three-Way Catalytic Converter with Mechanistic Kinetics Using the NewtonKrylov Method on a Parallel Computer," *Computers and Chemical Engineering*, vol. 26, no. 3, pp. 439–455, Mar. 2002.

[13] H. Santos and M. Costa, “Modelling Transport Phenomena and Chemical Reactions in Automotive Three-Way Catalytic Converters,” *Chemical Engineering Journal*, vol. 148, no. 1, pp. 173–183, May 2009.

[14] W. H. Ray, *Advanced Process Control.* New York: McGraw-Hill. Butterworths series in Chemical Engineering, 1989.

[15] H. Shang, J. F. Forbes, and M. Guay, “Model Predictive Control for Quasilinear Hyperbolic Distributed Parameter Systems,” *Industrial and Engineering Chemistry Research*, vol. 43, no. 9, pp. 2140–2149, Apr. 2004.

[16] L. Mohammadi, S. Dubljevic, and J. F. Forbes, “Robust Characteristic-Based MPC of a Fixed-Bed Reactor.” Marriott Waterfront, Baltimore, MD, USA: American Control Conference, 2010, pp. 4421–4426.

[17] H. Shang, J. Fraser Forbes, and M. Guay, “Feedback control of hyperbolic distributed parameter systems,” *Chemical Engineering Science*, vol. 60, no. 4, pp. 969–980, Feb. 2005.

[18] E. M. Hanczyc and A. Palazoglu, “Sliding Mode Control of Nonlinear Distributed Parameter Chemical Processes,” *Industrial and Engineering Chemistry Research*, vol. 34, no. 2, pp. 557–566, Feb. 1995.

[19] A. M. Fuxman, J. F. Forbes, and R. E. Hayes, “Characteristics-Based Model Predictive Control of a Catalytic Flow Reversal Reactor,” *Canadian Journal of Chemical Engineering*, vol. 85, pp. 424–432, 2007.

[20] P. Christofides and P. Daoutidis, “Finite-Dimensional Control of Parabolic PDE Systems Using Approximate Inertial Manifolds,” *Journal of Mathematical Analysis and Applications*, vol. 216, pp. 398–420, 1997.

[21] J. Baker and P. D. Christofides, “Finite-Dimensional Approximation and Control of Non-linear Parabolic PDE Systems,” *International Journal of Control*, vol. 73, no. 5, pp. 439–456, 2000.

[22] A. Armaou and P. D. Christofides, “Dynamic Optimization of Dissipative PDE Systems Using Nonlinear Order Reduction,” *Chemical Engineering Science*, vol. 57, pp. 5083–5114, 2002.

[23] S. Dubljevic, P. D. Christofides, and I. G. Kevrekidis, “Distributed Nonlinear Control of DiffusionReaction Processes,” *International Journal of Robust and Nonlinear Control*, vol. 14, no. 2, pp. 133–156, Jan. 2004.

[24] P. D. Christofides, “Robust Control of Parabolic PDE Systems,” *Chemical Engineering Science*, vol. 53, no. 16, pp. 2949–2965, Aug. 1998.

[25] S. Dubljevic and P. D. Christofides, “Predictive Output Feedback Control of Parabolic Partial Differential Equations (PDEs),” *Industrial and Engineering Chemistry Research*, vol. 45, pp. 8421–8429, 2006.

[26] S. Pitchaiah and A. Armaou, “Robust Control of Dissipative PDE Systems in the Presence of Uncertainty Using Adaptive Model Reduction.” Makedonia Palace, Thessaloniki, Greece: 17th Mediterranean Conference on Control & Automation, 2009, pp. 498–503.

[27] S. Dubljevic, P. Mhaskar, N. H. El-farra, and P. D. Christofides, “Predictive control of transport-reaction processes,” *Computers and Chemical Engineering*, vol. 29, no. 11-12, pp. 2335–2345, Oct. 2005.

[28] J. Ng and S. Dubljevic, "Optimal Boundary Control of a DiffusionConvection-Reaction PDE Model with Time-Dependent Spatial Domain: Czochralski Crystal Growth Process," *Chemical Engineering Science*, vol. 67, no. 1, pp. 111–119, Jan. 2012.

[29] R. F. Curtain and A. J. Pritchard, *Lecture Notes in Control and Information Sciences: Infinite Dimensional Linear Systems Theory.* Berlin-Heidelberg: Springer-Verlag, 1978.

[30] J. Ng, I. Aksikas, and S. Dubljevic, "Model Predictive Control Formulation for a Class of Time-Varying Linear Parabolic PDEs." O'Farrell Street, San Francisco, CA, USA: American Control Conference, 2011, pp. 2963–2968.

[31] M. Hsieh and J. Wang, "A Two-Cell Backstepping-Based Control Strategy for Diesel Engine Selective Catalytic Reduction Systems," *IEEE Transactions on Control Systems Technology*, vol. 19, no. 6, pp. 1504–1515, Nov. 2011.

[32] M. F. Hsieh and J. Wang, "Staircase Ammonia Coverage Ratio Profile Control for Diesel Engine Two-Cell Selective Catalytic Reduction Systems," no. x. Marriott Waterfront, Baltimore, MD, USA: American Control Conference, 2010, pp. 3003–3008.

[33] M. Hsieh and J. Wang, "Backstepping Based Nonlinear Ammonia Surface Coverage Ratio Control," no. x. Hollywood, California, USA: Proceedings of the ASME 2009 Dynamic Systems and Control Conference, 2009, pp. 1–8.

[34] M. Devarakonda, G. Parker, and J. H. Johnson, "Adequacy of Reduced Order Models for Model-Based Control in a Urea-SCR Aftertreatment System," vol. 2008, no. 724. Detroit, Michigan: World Congress, 2008, pp. 776–790.

[35] V. S. Maruthi Devarakonda, Gordon Parker and John H. Johnson and S. Santhanam, "Model-Based Estimation and Control System Development in a Urea-SCR Aftertreatment System," *SAE International Journal of Fuels and Lubricants.*, vol. 1, no. 1, pp. 646–661, 2008.

[36] C. M. Schär, C. H. Onder, H. P. Geering, and C. Constants, "Control of an SCR Catalytic Converter System for a Mobile Heavy-Duty Application," *IEEE Transactions on Control Systems Technology*, vol. 14, no. 4, pp. 641–653, 2006.

[37] C. T. Chen and W.-L. Tan, "Mathematical Modeling, Optimal Design and Control of an SCR Reactor for NOx Removal," *Journal of the Taiwan Institute of Chemical Engineers*, vol. 43, no. 3, pp. 409–419, May 2012.

[38] F. Willems and R. Cloudt, "Experimental Demonstration of a New Model-Based SCR Control Strategy for Cleaner Heavy-Duty Diesel Engines," *IEEE Transactions on Control Systems Technology*, vol. 19, no. 5, pp. 1305–1313, Sep. 2011.

[39] H. Krijnsen, J. van Leeuwen, R. Bakker, C. van den Bleek, and H. Calis, "Optimum NOx Abatement in Diesel Exhaust Using Inferential Feedforward Reductant Control," *Fuel*, vol. 80, no. 7, pp. 1001–1008, May 2001.

[40] D. Upadhyay and M. Van Nieuwstadt, "Model Based Analysis and Control Design of a Urea-SCR DeNOx Aftertreatment System," *Journal of Dynamic Systems, Measurement, and Control*, vol. 128, no. 3, p. 737, 2006.

[41] M. F. Hsieh and J. Wang, "Diesel Engine Selective Catalytic Reduction (SCR) Ammonia Surface Coverage Control Using a Computationally-Efficient Model Predictive Control Assisted Method," in *ASME 2009 Dynamic Systems and Control Conference*. Hollywood, California, USA: ASME, 2009, pp. 865–872.

[42] M. Meisami-azad, J. Mohammadpour, K. M. Grigoriadis, M. P. Harold, and M. A. Franchek, "LPV Gain-Scheduled Control of SCR Aftertreatment Systems," *International Journal of Control*, vol. 85, no. 1, pp. 114–133, 2012.

[43] A. Alizadeh Moghadam, I. Aksikas, S. Dubljevic, and J. F. Forbes, "Infinite-Dimensional LQ Optimal Control of a Dimethyl Ether (DME) Catalytic Distillation Column," *Journal of Process Control*, vol. 22, no. 9, pp. 1655–1669, Oct. 2012.

[44] A. Bensoussan, G. Da Prato, M. C.Delfour, and S. K.Mitter, *Systems and Control: Foundations and Applications, Representation and Control of Infinite-Dimensional Systems*. Boston: Birkhauser, 2007.

[45] A. Alizadeh Moghadam, I. Aksikas, S. Dubljevic, and J. F. Forbes, "Boundary Optimal (LQ) Control of Coupled Hyperbolic PDEs and ODEs," *Automatica*, vol. 49, no. 2, pp. 526–533, Feb. 2013.

[46] M. Krstic and A. Smyshlyaev, "Backstepping Boundary Control for First-Order Hyperbolic PDEs and Application to Systems with Actuator and Sensor Delays," *Systems and Control Letters*, vol. 57, no. 9, pp. 750–758, Sep. 2008.

[47] S. Tang and C. Xie, "State and Output Feedback Boundary Control for a Coupled PDEODE System," *Systems and Control Letters*, vol. 60, no. 8, pp. 540–545, Aug. 2011.

[48] M. Krstic and A. Smyshlyaev, *Boundary Control of PDEs A Course on Backstepping Designs*. SIAM, 2008.

[49] J. T. Betts, *Practical Methods for Optimal Control and Estimation Using Nonlinear Programming*, 2nd ed. SIAM, 2010.

[50] R. G. Rice and D. D.Do, *Applied Mathematics and Modeling for Chemical Engineers*. John Wiley & Sons, Inc., 1995.

[51] M. Li and P. D. Christofides, "Optimal Control of Diffusion-Convection-Reaction Processes Using Reduced-Order Models," *Computers and Chemical Engineering*, vol. 32, no. 9, pp. 2123–2135, Sep. 2008.

[52] S. E. El-gendi, "Chebyshev Solution of Differential, Integral and Integro-Differential Equations," *The Computer Journal*, pp. 282–287, 1969.

[53] T. El-Gindy, H. El-Hawary, M. Salim, and M. El-Kady, "A Chebyshev Approximation for Solving Optimal Control Problems," *Computers and Mathematics with Applications*, vol. 29, no. 6, pp. 35–45, Mar. 1995.

[54] M. El-Kady and E. M. Elbarbary, "A Chebyshev Expansion Method for Solving Nonlinear Optimal Control Problems," *Applied Mathematics and Computation*, vol. 129, no. 2-3, pp. 171–182, Jul. 2002.

[55] M. El-Kady, M. Salim, and A. El-Sagheer, "Numerical Treatment of Multiobjective Optimal Control Problems," *Automatica*, vol. 39, no. 1, pp. 47–55, Jan. 2003.

[56] J. Maciejowski, *Predictive Control with Constraints.* Prentice Hall, 2000.

[57] K. R. Muske and J. B. Rawlings, “Model Predictive Control with Linear Models,” *AIChE Journal*, vol. 39, no. 2, pp. 262–287, Feb. 1993.

[58] H. Chen and F. Allgower, “A Quasi-Infinite Horizon Nonlinear Model Predictive Control Scheme with Guaranteed Stability,” *Automatica*, vol. 34, no. 10, pp. 1205–1217, 1998.

[59] L. Grüne and A. Rantzer, “On the Infinite Horizon Performance of Receding Horizon Controllers,” *IEEE TRANSACTIONS ON AUTOMATIC CONTROL*, vol. 53, no. 9, pp. 2100–2111, 2008.

[60] L. Magni, D. M. Raimondo, and F. Allgöwer, *Nonlinear Model Predictive Control Towards New Challenging Applications.* Springer, 2009.

[61] P. Christofides, J. Liu, and D. M. de la Peña, *Networked and Distributed Predictive Control.* Springer, 2011.

[62] L. Grüne and J. Pannek, *Nonlinear Model Predictive Control Theory and Algorithms.* Springer, 2011.

[63] D. Q. Mayne, J. B. Rawlings, C. V. Rao, and P. O. M. Scokaert, “Constrained Model Predictive Control : Stability and Optimality,” *Automatica*, vol. 36, pp. 789–814, 2000.